

See discussions, stats, and author profiles for this publication at: <https://www.researchgate.net/publication/49687520>

Backbone Dynamics of Deoxy and Carbonmonoxy Hemoglobin by NMR/SRLS

ARTICLE *in* THE JOURNAL OF PHYSICAL CHEMISTRY B · JANUARY 2011

Impact Factor: 3.3 · DOI: 10.1021/jp107553j · Source: PubMed

CITATIONS

11

READS

34

4 AUTHORS, INCLUDING:



Mirco Zerbetto

University of Padova

35 PUBLICATIONS 314 CITATIONS

[SEE PROFILE](#)



Antonino Polimeno

University of Padova

124 PUBLICATIONS 1,552 CITATIONS

[SEE PROFILE](#)

Backbone Dynamics of Deoxy and Carbonmonoxy Hemoglobin by NMR/SRLS

Eva Meirovitch,^{*†} Mirco Zerbetto,[‡] Antonino Polimeno,[‡] and Jack H. Freed[§]

The Mina and Everard Goodman Faculty of Life Sciences, Bar-Ilan University, Ramat-Gan 52900, Israel; Department of Chemistry, University of Padua, 35131 Padua, Italy; and Baker Laboratory of Chemistry and Chemical Biology, Cornell University, Ithaca, New York 14853-1301, United States

Received: August 10, 2010; Revised Manuscript Received: November 15, 2010

The slowly relaxing local structure (SRLS) approach, developed for NMR spin relaxation analysis in proteins, is applied herein to amide ^{15}N relaxation in deoxy and carbonmonoxy hemoglobin. Experimental data including ^{15}N T_1 , T_2 and $^{15}\text{N}-\{\text{H}\}$ NOE, acquired at 11.7 and 14.1 T, and 29 and 34 °C, are analyzed. The restricted local motion of the N–H bond is described in terms of the principal value (S_0^2) and orientation (β_D) of an axial local ordering tensor, S , and the principal values (R_{\parallel}^L and R_{\perp}^L) and orientation (β_O) of an axial local diffusion tensor, R^L . The parameters c_0^2 (the potential coefficient in terms of which S_0^2 is defined), R_{\parallel}^L , β_D , and β_O are determined by data fitting; R_{\perp}^L is set equal to the global motional rate, R^C , found previously to be $(5.2-5.8) \times 10^6$ 1/s in the temperature range investigated. The principal axis of S is (nearly) parallel to the $C_{i-1}^{\alpha}-C_i^{\alpha}$ axis; when the two axes are parallel, $\beta_D = -101.3^\circ$ (in the frame used). The principal axis of R^L is (nearly) parallel to the N–H bond; when the two axes are parallel, $\beta_O = -101.3^\circ$. For “rigid” N–H bonds located in secondary structure elements the best-fit parameters are $S_0^2 = 0.88-0.95$ (corresponding to local potentials of 8.6–19.9 $k_B T$), $R_{\parallel}^L = 10^9-10^{10}$ 1/s, $\beta_D = -101.3^\circ \pm 2.0^\circ$, and $\beta_O = -101.3^\circ \pm 4^\circ$. For flexible N–H bonds located in loops the best-fit values are $S_0^2 = 0.75-0.80$ (corresponding to local potentials of 4.5–5.5 $k_B T$), $R_{\parallel}^L = (1.0-6.3) \times 10^8$ 1/s, $\beta_D = -101.3^\circ \pm 4.0^\circ$, and $\beta_O = -101.3^\circ \pm 10^\circ$. These results are important in view of their physical clarity, inherent potential for further interpretation, consistency, and new qualitative insights provided (vide infra).

I. Introduction

NMR spin relaxation is a powerful method for elucidating protein dynamics.^{1–13} The ^{15}N nucleus of the amide $^{15}\text{N}-\text{H}$ bond is typically used to study backbone dynamics,^{1–5,7–10} and the ^2H nucleus of the $^{13}\text{CDH}_2$ methyl group^{5,6,11–13} is used to study side-chain dynamics. We developed in recent years the slowly relaxing local structure (SRLS) approach^{14–16} for analyzing NMR spin relaxation in proteins.^{17–19} SRLS has been implemented so far as a two-body coupled-rotator model which accounts for dynamical coupling between the local motion of the NMR probe and the global motion of the protein, and allows for general properties of the second-rank tensors involved. Here, we focus on ^{15}N spin relaxation in the deoxy and carbonmonoxy forms of normal adult hemoglobin, in short Hb A and HbCO A, analyzed with SRLS. Experimental data including ^{15}N T_1 , T_2 and $^{15}\text{N}-\{\text{H}\}$ NOE, acquired previously at 11.7 and 14.1 T, and 29 and 34 °C,²⁰ are used.

Hemoglobin is involved in oxygen binding, transport, and release in the tissue to myoglobin for storage. Subsequently, it binds CO_2 in the tissue and transports it to the lungs for release. The oxygenation of hemoglobin is regulated by homotropic interactions among its binding sites, and heterotropic interactions between individual amino acids in the protein and various effectors. Hb A has a molecular weight of approximately 64.5 kDa. The molecule comprises two identical α -chains and two identical β -chains. The former consist of 141 amino acids, and the latter of 146 amino acids.²¹ Two (classical) quaternary

structures — the T (tense) form for low-affinity deoxy-Hb, and the R (relaxed) form for high-affinity oxy-Hb — were determined.²² A quaternary structure called R2 was also reported.^{23,24} Structural transitions, referred to as T-to-T_{high} quaternary transitions, have been identified based on crystallographic structures of mutants.²⁵

Approximately 80% of the backbone resonances of HbCO A (which can be considered a mimic of oxyhemoglobin) have been assigned;²⁶ samples wherein the α - and β -chains were specifically (^2H , ^{15}N , ^{13}C)-labeled²⁷ were used. A residual dipolar coupling (RDC) study of the amide bonds of HbCO A has shown that this molecule prevails in solution as an intermediate between the crystal structures R and R2.²⁶ Exchange broadening at the subunit interface indicates that rapid equilibrium between different conformations, most likely including R and R2, prevails.²⁶ Clearly, this scenario differs from the single-conformation crystallographic description.²² There is evidence, also based on RDC measurements, that the solution structure of Hb A may also differ from its crystal structure.²⁸

Dynamic features of Hb A and HbCO A have been characterized by various studies.^{20,29–34} Of particular relevance is the investigation of backbone dynamics using ^{15}N amide spin relaxation,²⁰ analyzed with the traditional model-free (MF) approach. Model-free^{35–37} a simple method which ignores mode coupling and can treat only simple tensorial properties within the scope of physical parameters. However, the actual cases are not simple, and the experimental data are sensitive to their complexity (see below). MF has coped with this situation (implicitly) by “generalizing” its parameters. In most cases the data can be fit statistically, albeit with inaccurate parameters, which have absorbed unaccounted for factors. SRLS can be

^{*} Corresponding author. E-mail: eva@nmrsg5.ls.biu.ac.il. Phone: 972-3-531-8049. Fax: 972-3-738-4058.

[†] Bar-Ilan University.

[‡] University of Padua.

[§] Cornell University.

considered the generalization of MF, yielding the latter in the simple limits in which MF features physical parameters.^{17–19}

Squared MF generalized order parameters, S^2 , with an average value of 0.85 have been determined for “rigid” N–H bonds residing in the well-structured regions of the polypeptide chains of Hb A and HbCO A. Values of 0.75 on average have been determined for N–H bonds residing in loops. These results are typical of globular proteins (e.g., cf. ref 8).

The effective MF local motional correlation times, τ_e , expected to equal several tens of picoseconds for the rigid N–H bonds, and several hundreds of picoseconds for the flexible N–H bonds,⁸ yielded a puzzling picture. For example, for the α -chain of Hb A examined at 29 °C, τ_e was found to be in the 3–40 ps range for 33% of the residues, in the 200–10 000 ps range for 25% of the residues, and zero for 42% of the residues. Slow local motions correlate with small NOEs (e.g., cf. ref 8). Relatively small experimental NOEs were observed for the N–H bonds of residues H20, R31, G51, and M76. Yet, their τ_e values were found to be zero, or close to zero. On the other hand, most N–H bonds with large τ_e values (e.g., those pertaining to residues A13–G15, L34–F36) are located in helices. In the segment S49–A53 the τ_e values were found to alternate between 10 ns and 20 ps. Effective local motional correlation times can be very inaccurate; in some cases they are not even reported. This point of view was adopted in ref 20. On the other hand, quite a few conformational exchange terms, R_{ex} , determined with MF data fitting,³⁸ were considered informative.²⁰ Yet, in a later study, where conformational exchange mapping of Hb A and HbCO A was carried out,³⁴ it turned out that most of the MF-determined R_{ex} terms are artificial.

The problematic nature of some parameters (τ_e and R_{ex}) necessarily affects in an adverse manner the accuracy of the remaining parameters (S^2). Yet, S^2 was used to characterize residues known to be involved in the regulation of oxygen binding in general and the allosteric phenomenon in particular. They include residues α 31 (R), β 3 (L), β 41 (F), β 109 (V), β 123 (T), and β 146 (H).²⁰ If S^2 is inaccurate, the important information it provides on changes induced at these sites upon CO binding to Hb will also be inaccurate. The question is whether data imperfection, or oversimplified analysis, is responsible for this unsatisfactory state of affairs. We address this matter herein by using enhanced SRLS analysis. Unlike MF, SRLS accounts for dynamical coupling and general tensorial properties. Based on previous work, mode coupling is likely to affect the analysis of flexible N–H bonds, and have a small effect on the analysis of rigid N–H bonds.^{18,19} On the other hand, low symmetry of the local spatial restrictions, and general features of the local geometry, are properties akin to all the N–H sites in proteins.^{18,19,39–44} The question is whether the experimental ^{15}N relaxation parameters of Hb A and HbCO A are sensitive to these properties.

We have found previously that the experimental data of N–H bonds residing in internally mobile domains are sensitive to general tensorial properties.^{18,19,45–49} The local potentials at these N–H sites were found to be rhombic, with the Z-axes of the local ordering tensors (defined in terms of these potentials) being parallel to the C_{i-1}^α – C_i^α axes.^{18,19,45–49} For practical reasons, it was not possible in the past to analyze rigid N–H bonds with this scenario. Using the computer programs available at that time,¹⁸ the calculations were very tedious in the limit of large time scale separation between the local and global motions, and rhombic potentials, characteristic of rigid N–H bonds. Recently, we developed a theoretical/computational tool which is 10 times faster than our previous program,¹⁸ and more general with regard

to tensorial properties.⁵⁰ In particular, the local ordering and the local diffusion frames can be separated in the new formulation,⁵⁰ while for simplicity they were taken as being the same in the older formulation.¹⁸ As shown below, we found that this feature is particularly useful.

The local ordering and the local diffusion are different physical properties. For an N–H bond attached physically to the protein, they are determined by the structural properties of the immediate protein surroundings and the hydrodynamic properties of the probe. The local ordering is likely to be affected to a larger extent by the immediate protein surroundings and to a smaller extent by the hydrodynamic properties of the probe. The local diffusion is likely to be affected to a larger extent by the hydrodynamic properties of the probe and to a smaller extent by the immediate protein surroundings. The relative contribution of these factors is expected to differ from site to site.

We model this scenario in terms of arbitrarily tilted axial local ordering and local diffusion tensors, and determine their principal values and orientations by data fitting. Together with the magnetic tensors (which are also allowed to be tilted arbitrarily),⁵⁰ a realistic and physically sound description emerges. In this representation, the asymmetry of the local spatial restrictions is implicit in the tilted tensor frames and the principal values of the various tensors. As before,^{18,19,45–49} we found that this asymmetry has to be accounted for if one wishes to extract properly the information inherent in the experimental data. The respective calculations are very efficient (see below).

SRLS is general enough to provide a realistic description of N–H bond dynamics in proteins. Other treatments, e.g., the 3D Gaussian axial fluctuations model,³⁹ and the network of coupled rotators model,⁴⁴ which have been applied to spin relaxation in proteins, have the local geometry encoded, do not provide site-specific motional rates (let alone local motional tensors), and consider all the magnetic tensors axial and collinear.

The results presented here for Hb A and HbCO A differ substantially from the previous MF analysis,²⁰ which led to the puzzling picture noted above. Our SRLS analysis provides a consistent picture based on physically well-defined parameters, which applies to both rigid and flexible N–H bonds, and is free of artificial R_{ex} terms. This indicates that the SRLS enhancements are required. We show below that the model we suggest matches data sensitivity.

Another challenge is to correlate the mesoscopic information obtained with spin relaxation analysis with atomistic descriptions of the site of the motion of the probe. For that, joint spin relaxation and molecular dynamics (MD) studies, and integration with quantum chemical approaches, are required. Such developments have been pursued by some of us in different contexts.^{51–60} Efforts to develop similar methods for NMR relaxation in proteins are in progress.⁶¹

The article is structured as follows. A Theoretical Summary is provided. The subsequent Results and Discussion section comprises a detailed SRLS analysis of ^{15}N spin relaxation parameters from Hb A and HbCO. The article ends with Conclusions.

2. Theoretical Summary

2.1. Slowly Relaxing Local Structure Approach. The fundamentals of the stochastic coupled rotator slowly relaxing local structure theory, as applied to NMR spin relaxation in proteins, have been presented and reviewed previously.^{17–19} A brief summary is given below for convenience.

The various reference frames that define the SRLS model are shown in Figure 1a. They are related to the N–H bond as

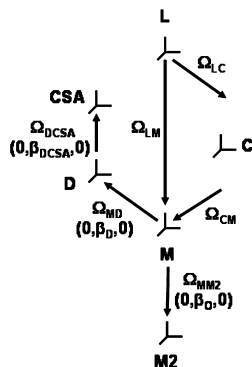


Figure 1. Various reference frames that define the SRLS model. L is the laboratory frame; C is the global diffusion frame; M is the local ordering frame fixed in the N–H bond; M2 is the local diffusion frame fixed in the N–H bond; D is the magnetic ^{15}N – ^1H dipolar frame and CSA the magnetic ^{15}N chemical shift anisotropy frame, both fixed in the N–H bond. The Euler angles Ω_{LC} are modulated by the global tumbling; the Euler angles Ω_{LM} are modulated by the local and global motions; in relative (probe versus protein) coordinates, the Euler angles Ω_{CM} are modulated by the local motion.

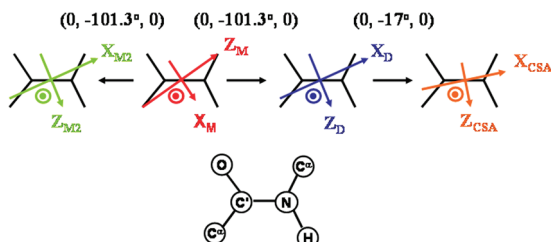


Figure 2. Schematic drawing showing the axial M, M2, D, and CSA frames in the context of the peptide-bond plane. Z_D lies along N–H; Y_D and Y_{CSA} are perpendicular to the peptide-bond plane.^{62,63} The axes X_{CSA} , Y_{CSA} , and Z_{CSA} are defined to be aligned with the most shielded (σ_{11}), intermediate (σ_{22}), and least shielded (σ_{33}) components of the ^{15}N shielding tensor, respectively.^{62,63} Z_M is taken to be parallel to the C_{i-1}^α – C_i^α axis, and Z_{M2} is taken to be parallel to the N–H bond. The rotations follow the ZYZ convention.

the probe. The laboratory L frame is space-fixed with its Z-axis aligned along the external magnetic field, B_0 . The global diffusion frame, C, is fixed in the protein. In this study, we consider isotropic global diffusion. In this case, the C frame is the same as the local director frame, which is parallel to the equilibrium orientation of the N–H bond. M is the coordinate frame in which the local ordering tensor is diagonal, and M2 is the coordinate frame in which the local diffusion tensor is diagonal. They are both fixed in the probe.

The magnetic ^{15}N – ^1H dipolar tensor frame, D, and the magnetic ^{15}N CSA tensor frame CSA, are fixed in the probe. The Euler angles for rotation from M to D are given by Ω_{MD} from M to M2 by Ω_{MM2} , and from D to CSA by Ω_{DCSA} . Their values may be derived based on stereochemical considerations or determined by data fitting (the orientations of the magnetic tensors are assumed to be known^{62,63} in this study). In Figure 2 we depict the scenario in which the D, M, and M2 frames are axially symmetric, the principal axis of the local ordering tensor is parallel to the C_{i-1}^α – C_i^α axis, and the principal axis of the local diffusion tensor is parallel to the N–H bond. In this case, one has $\Omega_{MD} = (0, \beta_{MD}, 0) = (0, -101.3^\circ, 0)$, and $\Omega_{MM2} = (0, \beta_{MM2}, 0) = (0, -101.3^\circ, 0)$. We denote below β_{MD} as β_D , and β_{MM2} as β_0 .

The time-dependent Euler angles, $\Omega_{LM}(t)$, are modulated by the local and global motions. The time-dependent Euler angles $\Omega_{LC}(t)$ are modulated by the global tumbling. For describing

the local motion, we use a relative (probe versus protein) coordinate scheme; that is, $\Omega_{CM}(t) = \Omega_{LM}(t) - \Omega_{LC}(t)$.^{18,19,50} The two rotators are coupled by the potential of mean torque (POMT), $U(\Omega_{CM})$. The diffusion equation for the coupled system is given by

$$\frac{\partial}{\partial t} P(X, t) = -\hat{\Gamma} P(X, t) \quad (1)$$

where X is a set of coordinates completely describing the system. One has^{18,19,50}

$$\begin{aligned} X &= (\Omega_{CM}, \Omega_{LC}) \\ \hat{\Gamma} &= \hat{J}(\Omega_{CM}) \mathbf{R}_{eq}^L \hat{J}(\Omega_{CM}) P_{eq}^{-1} + [\hat{J}(\Omega_{CM}) - \hat{J}(\Omega_{LC})] \\ &\quad \mathbf{R}_{eq}^C [\hat{J}(\Omega_{CM}) - \hat{J}(\Omega_{LC})] P_{eq}^{-1} \end{aligned} \quad (2)$$

where $\hat{J}(\Omega_{CM})$ and $\hat{J}(\Omega_{LC})$ are the infinitesimal rotation operators for the probe and the protein, respectively.

The Boltzmann distribution is $P_{eq} = \exp[-U(\Omega_{CM})/k_B T]/\langle \exp[-U(\Omega_{CM})/k_B T] \rangle$. The potential $U(\Omega_{CM})$ is in general expanded in the full basis set of the Wigner rotation matrix elements. When only the $L = 2$ terms are preserved, one has^{18,19,50}

$$U(\Omega_{CM}) = \frac{U(\Omega_{CM})}{k_B T} \approx -c_0^2 D_{0,0}^2(\Omega_{CM}) - c_2^2 [D_{0,2}^2(\Omega_{CM}) + D_{0,-2}^2(\Omega_{CM})] \quad (3)$$

The coefficient c_0^2 is related to the strength of the POMT, and c_2^2 is related to its nonaxiality. The order parameters, $S_0^2 = \langle D_{00}^2(\Omega_{CM}) \rangle$ and $S_2^2 = \langle D_{02}^2(\Omega_{CM}) + D_{0-2}^2(\Omega_{CM}) \rangle$, are calculated from c_0^2 and c_2^2 according to^{18,19,50}

$$\begin{aligned} \langle D_{0n}^2(\Omega_{CM}) \rangle &= \int d\Omega_{CM} D_{0n}^2(\Omega_{CM}) \times \\ &\quad \exp[-u(\Omega_{CM})] / \int d\Omega_{CM} \exp[-u(\Omega_{CM})] \end{aligned} \quad (4)$$

The Cartesian ordering tensor components are given by $S_{zz} = S_0^2$, $S_{xx} = (\sqrt{(3/2)}S_2^2 - S_0^2)/2$, $S_{yy} = -(\sqrt{(3/2)}S_2^2 + S_0^2)/2$, with $S_{xx} + S_{yy} + S_{zz} = 0$.

Expansion terms corresponding to $L = 4$, $K = 0, 2, 4$, (c_0^4 , c_2^4 , and c_4^4) are included in our most recent computational scheme.⁵⁰ They allow a more detailed modeling, in particular diffusion within two wells with less frequent jumps between them.^{15,64} More general multipotential-well models may be included by adding appropriate terms in the expansion of $U(\Omega_{CM})$. This is relevant for more complex dynamics.

Equation 2 is solved to yield the SRLS time correlation functions which lead by Fourier transformation to the spectral densities, $j_{K,K'}(\omega) = \sum_i (c_{K,K',i} \tau_i) / (1 + \omega^2 \tau_i^2)$.^{18,19,50} The relevant pairs, K, K' , are determined by the symmetry of the local ordering/local diffusion and magnetic tensors (in this study only the $K, K' = 0, 0; 1, 1; 2, 2$ contributions are relevant). In practice, a finite number of terms is sufficient for numerical convergence of the solution.

The $j_{K,K'}(\omega)$ functions are assembled into the measurable spectral densities according to the local geometry.⁶⁵ Here the relevant functions are J^{DD} and J^{CC} , where “D” denotes the ^{15}N – ^1H dipolar interaction and “C” the ^{15}N –CSA interaction.

J^{DD} depends on the Euler angles Ω_{MD} . $J^{CC}(\omega)$ is calculated from $J^{DD}(\omega)$; it depends on the Euler angles Ω_{MD} and Ω_{DCSA} . In calculating $J^{CC}(\omega)$, all three functions, $j_{KK}(\omega)$, are required. MF features only $J(\omega) = j_{00}(\omega)$;^{17–19} therefore, one has to set $J^{CC}(\omega) = J^{DD}(\omega) = J(\omega)$.³⁵

For an axial POMT and an axial dipolar tensor, the function $J^{DD}(\omega)$ is given by¹⁷

$$J^{DD}(\omega) = (d_{00}^2(\beta_D))^2 j_{00}(\omega) + 2(d_{10}^2(\beta_D))^2 j_{11}(\omega) + 2(d_{20}^2(\beta_D))^2 j_{22}(\omega) \quad (5)$$

The ^{15}N relaxation parameters T_1 , T_2 , and $^{15}\text{N}-\{^1\text{H}\}$ NOE are calculated as a function of $J^{DD}(0)$, $J^{DD}(\omega_H)$, $J^{DD}(\omega_N)$, $J^{DD}(\omega_H - \omega_N)$, $J^{DD}(\omega_H + \omega_N)$, $J^{CC}(0)$, $J^{CC}(\omega_N)$, and the magnetic interactions, using standard expressions for NMR spin relaxation.^{66,67}

In addition to the enhancements to the POMT mentioned above, our most recent fitting scheme⁵⁰ allows separating the local ordering and the local diffusion tensor frames, and allows for rhombic local (\mathbf{R}^L) and global (\mathbf{R}^C) diffusion tensors. Importantly, the SRLS program has been integrated with a hydrodynamics-based approach for calculating anisotropic \mathbf{R}^C tensors.⁶⁸ The programming language used is C++ (previously¹⁸ we used the FORTRAN programming language). The compute-intensive parts of the code have been parallelized, and object-oriented programming has been used. These features brought about an increase in efficiency of approximately one order of magnitude relative to the fitting scheme developed in ref 18.

We call this software package C++OPPS (COupled Protein Probe Smoluchowski).⁵⁰ C++OPPS is distributed under the GNU Public License (GPL) v2.0. The software is available at the Web site <http://www.chimica/unipd.it/licc/software.html>.

2.2. Model-Free. The MF approach uses $J(\omega) = J^{DD}(\omega) = J^{CC}(\omega)$, made of two Lorentzian terms which represent the global motion and a single (effective) local motion.^{35,36} This simple form is based on the premise that these motions are statistically independent, or “decoupled”, because they are time scale separated.³⁵ Implicitly, all the tensorial properties are simple: the global diffusion is isotropic, the local motion is isotropic, the local ordering is axial, and its principal axis is collinear with the principal axes of all the magnetic tensors involved. The MF spectral density is given by³⁵

$$J(\omega) = S^2 \tau_m / (1 + \tau_m^2 \omega^2) + (1 - S^2) \tau_e' / (1 + \tau_e'^2 \omega^2) \quad (6)$$

The parameter τ_m is the correlation time for the global motion, and $\tau_e \ll \tau_m$ is the effective correlation time for the local motion. By virtue of $\tau_e \ll \tau_m$, one has $1/\tau_e' = 1/\tau_m + 1/\tau_e \sim 1/\tau_e$. S^2 is defined as the plateau value, $C^L(\infty)$, to which the local motional time correlation function, $C^L(t)$, is assumed to converge at long times. Mathematically, $C^L(\infty)$ is given by

$$\sum_{m=0,\pm 1,\pm 2} \langle |Y_{2m}(\theta, \phi)|^2 \rangle$$

where Y_{2m} are the spherical harmonics of Brink and Satchler.⁶⁹ A “generalized” order parameter is defined as $S \equiv \sqrt{(C^L(\infty))}$.³⁵ S^2 is considered to represent the amplitude of the local motion. In the context of the physical definition of order parameters (eqs 3 and 4), this is appropriate in the limit of a strong axial POMT and local motion in the extreme motional narrowing

limit.¹⁶ Based on the theory of moments, τ_e is defined as the area of the exact time correlation function for internal motion (corresponding to a “frozen” protein³⁵) divided by $(1 - S^2)$.

The extended MF (EMF) spectral density³⁷ features a fast local motion, with effective correlation time, τ_f , and squared order parameters, S_f^2 , and a slow local motion, with effective correlation time, τ_s , and squared order parameter, S_s^2 . All three dynamic modes, represented by τ_m , τ_f , and τ_s , are assumed to be decoupled from one another. In practice, τ_s and τ_m are allowed to occur on the same time scale.

3. Results and Discussion

3.1. Examination of the Parameters Range Corresponding to Large Proteins. N–H bonds residing in internally mobile protein domains, which reorient on the same time scale as the global motion, have been investigated with a SRLS parameter combination shown to match data sensitivity.^{18,19,49} Here we apply another SRLS parameter combination to the N–H bonds of large proteins, Hb A and HbCO A, which comprise mainly rigid N–H bonds, and a limited number of flexible N–H bonds located in relatively small loops. The parameter range corresponding to these systems is likely to be different from the parameter range corresponding to medium-size proteins with internally mobile domains. We start our analysis with a sensitivity test of the parameter range corresponding to Hb A and HbCO A.

Hb A (HbCO A) reorients in solution with correlation times, τ_m , of 32.8 and 29.0 (32.0 and 27.9) ns at 29 and 34 °C, respectively.²⁰ For $\tau = 1/(6R^L)$ values of tens of picoseconds (e.g., cf. ref 8), the expected time scale separation, τ/τ_m , is on the order of 10^{-3} . In Table 1 we compare SRLS and MF data-fitting calculations carried out in this parameter range for typical parameter combinations. The spin relaxation data of residue N9 of the α -chain of Hb A, acquired at 11.7 and 14.1 T, and 29 °C,²⁰ are used as an example. The various columns of Table 1 show c_0^2 (the coefficient of the axial local potential), S_0^2 (the corresponding order parameter), its square, β_D (the tilt angle between the principal axes of the local ordering and dipolar tensor frames), β_O (the tilt angle between the principal axes of the local ordering and local diffusion tensor frames), R_{ex} (the conformational exchange term),³⁸ and χ^2/df . The parameter df denotes the number of degrees of freedom. One has $\text{df} = 5$ for calculations 1–3, $\text{df} = 4$ for calculations 4 and 5, $\text{df} = 3$ for calculation 6, and $\text{df} = 2$ is for calculation 7. The 0.05 critical values of χ^2/df for $\text{df} = 2, 3, 4$, and 5 are 5.99, 7.81, 9.49, and 11.1, respectively. The 0.1 critical values of χ^2/df for $\text{df} = 2, 3, 4$, and 5 are 4.61, 6.25, 7.78, and 9.24, respectively.⁷⁰ All of the χ^2/df values in Table 1 are below the 0.05 critical values; hence all the corresponding results are considered appropriate from a statistical point of view. They still need to fulfill the criterion of physical viability.

All the calculations shown in Table 1 used a bond length $r_{NH} = 1.02$ Å and a ^{15}N CSA value of –172 ppm (e.g., cf. ref 50). $R^C = 5.08 \times 10^6$ 1/s, determined in ref 20 to be the rate of isotropic global motion of Hb A at 29 °C, was used. In calculation 1 (SRLS), only the parameter c_0^2 was allowed to vary. $R^L = 5.08 \times 10^{10}$ 1/s, $\beta_D = \beta_O = 0^\circ$, and $\beta_{DCSA} = 0^\circ$ were preset. R^L is larger than R^C by 4 orders of magnitude; hence $\tau^L = 1/(6R^L)$ is virtually negligible. The parameter S_0^2 was calculated from c_0^2 (cf. eqs 3 and 4). In calculation 2 (MF) the parameter S^2 , formally analogous to the SRLS parameter (S_0^2)², was allowed to vary. In MF the values of β_D , β_O , and β_{DCSA} are implicitly zero. The parameter c_0^2 was calculated from $S \rightarrow S_0^2$

TABLE 1: Results of Data Fitting Calculations Carried out for Residue N9 of the α -Chain of Hb A^a

calcd	c_0^2	S_0^2	$(S_0^2)^2$	R^L (1/s)	β_{DCSA} (deg)	β_D^b (deg)	β_O^b (deg)	R_{ex}^b (1/s)	χ^2/df
1	19.2	0.947	0.896	5.08×10^{10}	0.0	0	0	0	2.0
2	19.3	0.948	0.898^c	$\rightarrow \infty$	0.0	0	0	0	11.2
3	22.7	0.955	0.912	5.08×10^{10}	-17	0	0	0	4.5
4	27.3	0.963	0.927	2.2×10^{10}	-17	0	0	0	4.4
5	19.5	0.947	0.897^c	1.0×10^{11}	0.0	0	0	0	11.0
6	20.3	0.950	0.903	2.3×10^{10}	-17	0	0	2.6	0.9
7	9.6	0.891	9.794	5.9×10^{10}	-17	-98.7	-95.5	0	1.0

^a The experimental data were acquired at 29 °C and 11.7 and 14.1 T.²⁰ The input parameters are specified in the text. The best-fit parameter values are typed in bold-face. In SRLS potential coefficients are varied and order parameters are calculated from them. Calculations 1, 3, 4, 6, and 7 used SRLS; calculations 2 and 5 used MF. The SRLS rates are “renormalized” rates, given by $R^L \times c_0^2/2$.^{72,73} The parameter df in the last column denotes the number of degrees of freedom: df = 5 for calculations 1–3, df = 4 for calculations 4 and 5, df = 3 for calculation 6, and df = 2 is for calculation 7. The 0.05 critical values of χ^2/df for df = 2, 3, 4, and 5 are 5.99, 7.81, 9.49, and 11.1, respectively. The 0.1 critical values of χ^2/df for df = 2, 3, 4, and 5 are 4.61, 6.25, 7.78, and 9.24, respectively.⁷⁰ Further details are given in the text. ^b In all the cases except for R_{ex} in calculation 6, and β_O and β_D in calculation 7, the values of these parameters were fixed at zero. ^c The fitted parameter in the MF calculations is S^2 . Assuming that S represents S_0^2 , the potential coefficient, c_0^2 , was calculated from S using eqs 3 and 4. ^d This value represents R_{\perp}^L ; R_{\parallel}^L was set equal to R^C in calculation 7.

according to eqs 3 and 4. Calculation 2 is called “model 1” in MF;³⁸ calculation 1 (SRLS) is formally analogous to calculation 2 (MF).

Calculation 3 (SRLS) differs from calculation 1 (SRLS) in the angle β_{DCSA} being preset to -17° , which is its correct value (e.g., cf. ref 50). In calculation 4 (SRLS) c_0^2 and R^L were allowed to vary. The values of $\beta_D = \beta_O = 0^\circ$ and $\beta_{DCSA} = -17^\circ$ were preset. The SRLS local motional rate, which is the formal analogue of $1/(6\tau_e)$, is $R_{ren}^L = R^L \times c_0^2/2$.^{72,73} Its value, $R_{ren}^L = 3.0 \times 10^{11}$ 1/s, was calculated from the best-fit values of R^L and c_0^2 . Calculation 4 (SRLS) is the formal analogue of “model 2” MF,³⁸ which is represented by calculation 5 (MF). In the latter, S^2 (the formal analogue of $(S_0^2)^2$) and τ_e (the formal analogue of $\tau_{ren} = (1/6R_{ren}^L)$) were allowed to vary. The values of β_D , β_O , and β_{DCSA} are implicitly zero. The parameter c_0^2 was calculated from $S \rightarrow S_0^2$ according to eqs 3 and 4. Calculation 6 (SRLS) is the extension of calculation 4 (SRLS) where the conformational exchange term, R_{ex} , was also allowed to vary. Calculation 6 is the formal analogue of “model 4” MF.³⁸ The parameter $R_{ren}^L = 2.3 \times 10^{11}$ 1/s was calculated from the best-fit values of R^L and c_0^2 .

Calculation 7 differs fundamentally from calculations 1–6 in the way in which it treats the symmetry and orientation of the local ordering tensor, S , and the local diffusion tensor, R^L . As before, we vary c_0^2 . Unlike before, we take the R^L tensor to be axially symmetric: R_{\perp}^L is set equal to R^C and R_{\parallel}^L is allowed to vary. The angles β_D and β_O are allowed to vary from starting values of -101.3° , i.e., from the principal axis of S being parallel to $C_{i-1}^\alpha - C_i^\alpha$ and the principal axis of R^L being parallel to N–H (Figure 2). This orientation of S was determined in previous work for N–H bonds located in internally mobile domains;^{18,19,49} it is implicit in the model of ref 39. As pointed out below, the angles β_D and β_O stayed in most cases close to their starting values. The extent of their deviation from the latter embodies the complexity of the local ordering and the local motion.

The results obtained with calculation 7 differ substantially from the results obtained with calculations 1–6. All the SRLS calculations shown in Table 1 are appropriate from a statistical point of view. Only the “new model”, implemented in calculation 7, yields the important anisotropy of the local spatial restraints,^{18,19,39–44,39} and allows for general features of local geometry, found to be important.^{18,19,39–41,43,47} In particular, only this model yields the previously detected peptide-plane motion around $C_{i-1}^\alpha - C_i^\alpha$.^{18,19,39,40,47} Thus, out of the various models illustrated in Table 1, only the “new model” provides a

physically appropriate (and computationally effective) description of N–H bond dynamics in Hb A and HbCO A, which matches data sensitivity. Therefore, we selected this model for final data fitting.

The following can be concluded. MF agrees with SRLS when the local motion does not affect the analysis, and only a single irreducible magnetic tensor component enters the calculation (calculations 1 and 2). To obtain accurate squared order parameters, it is important to account for the dipolar-to-CSA tilt (calculations 1 and 3). The error in the squared order parameters of calculations 1 and 2 relative to the squared order parameter of calculation 3 is 1.75%; the error in the corresponding c_0^2 value is 15.4%. The large error in c_0^2 is a consequence of the functional form of the S^2 versus c_0^2 for large S^2 — e.g., see Figure 3 of ref 19. Not accounting for the D-to-CSA tilt has an adverse effect on the accuracy of the conformational entropy often derived from S^2 , as in this calculation c_0^2 (or a similar potential coefficient) is required.^{74–76}

The comparison between corresponding local motional rates in calculations 4 and 5 is carried out as follows. The local motional correlation time is given in calculation 4 within a good approximation by the renormalized correlation time, $\tau_{ren} \sim 2\tau/c_0^2$; the corresponding MF quantity is τ_e . Renormalization of τ by strong potentials was studied previously by Freed et al.^{72,73} in the context of a spin-bearing particle reorienting in a strong static potential exerted by a locally ordered medium. This model is analogous to the limiting case of SRLS, and the original MF approach, where $R^L \gg R^C$ implies a global diffusion axis, C, that reorients only over a much longer time scale. It was shown^{72,73} that for a highly ordered prolate top the relaxation of a nonequilibrium orientation happens by the molecular z axis (Z_M in SRLS) being rapidly restored to the director axis (C in SRLS). The respective correlation time, denoted τ_{ren} , is given by $\tau_{ren} = 2\tau/c_0^2 = 1/(3c_0^2 R^L)$.

Within the scope of SRLS, the results for a frozen C frame can be analyzed by a Born–Oppenheimer type approximation, where one first solves for the fast local motion for frozen global motion. We found previously that in the $R^L \gg R^C$ limit the SRLS spectral density comprises within a good approximation a main local motional term with eigenvalue that agrees with $1/\tau_{ren} \sim c_0^2/2\tau$, and a corresponding weighting factor of $1 - (S_0^2)^2$.¹⁸

Based on Table 1 one obtains $R_{ren}^L = 3.0 \times 10^{11}$ 1/s and $1/(6\tau_e) = 1.0 \times 10^{11}$. This large difference stems from the fact that (1) the MF formula used in calculation 5, and the SRLS spectral density used in calculation 4, differ, and (2) “model 2” is itself an approximation (see below). For ordering tensor symmetry

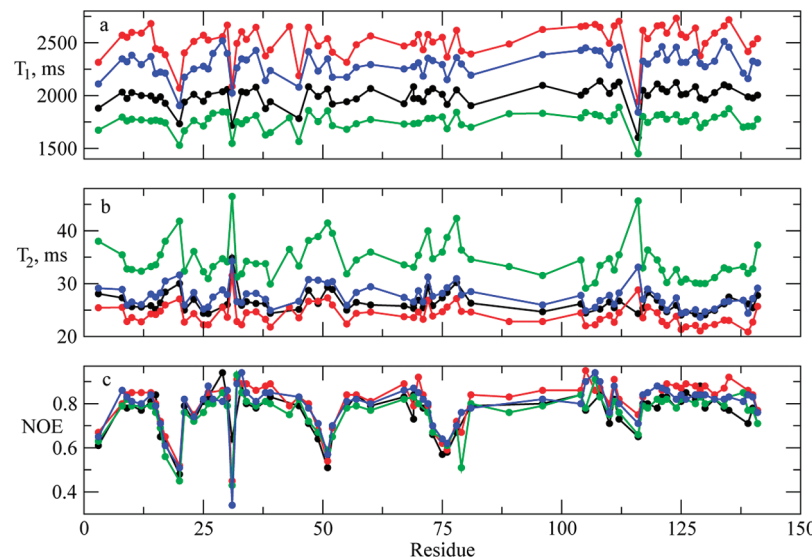


Figure 3. Experimental ^{15}N T_1 , T_2 and $^{15}\text{N}-\{\text{H}\}$ NOE acquired at 11.7 T and 29 °C (black), 14.1 T and 29 °C (red), 11.7 T and 34 °C (green), and 14.1 T and 34 °C (blue) for the α -chain of Hb A.²⁰

TABLE 2: Relaxation Parameters ^{15}N T_1 , T_2 and $^{15}\text{N}-\{\text{H}\}$ NOE Obtained As Outlined in the Text^a

calculation	^{15}N T_1 (s)	^{15}N T_2 (s)	$^{15}\text{N}-\{\text{H}\}$ NOE	% difference
1	2.710	0.0283	0.7496	
2. $R_{ }^C/R_{\perp}^C = 1.1$	2.678	0.0287	0.7505	-1.1, +1.4, +0.1
3. $R_{ }^C/R_{\perp}^C = 1.5$	2.281	0.0367	0.7616	-15.8, +18.8, +1.6
4. $R_{ }^C/R_{\perp}^C = 2.0$	2.200	0.0340	0.7638	-18.8, +20.1, +18.9

^a The numbers in the last column represent the percent difference in ^{15}N T_1 , T_2 and $^{15}\text{N}-\{\text{H}\}$ NOE relative to the corresponding data obtained in calculation 1.

other than axial prolate symmetry, an analytical formula for relating τ to a renormalized value does not exist. The differences between corresponding local motional rates might be larger than estimated above, and might vary significantly from site to site. The local motional correlation time, τ_e , absorbs unaccounted for factors in different ways at different sites and at different temperatures. Consequently, it is often inconsistent with the structural context (see above discussion on the τ_e values obtained for the α -chain of Hb A at 29 °C); typically it does not obey an Arrhenius relation. To our knowledge, the only published MF-based study where activation energies for local motion have been reported is ref 77, which relates to methyl dynamics in proteins. Only limited information for a small number of methyl groups, studied over a narrow temperature range, was obtained.

Calculation 6 shows the results obtained when the conformational exchange term, R_{ex} , was also allowed to vary. It can be seen that it is quite easy to obtain artificial R_{ex} contributions (cf. refs 20 and 34 with regard to Hb A and HbCO A) when only statistical criteria are used for the acceptance of results.

Calculation 7 sets forth a description of N–H bond dynamics in proteins which has not been used previously. We refer to it as the “new model”, used in all the calculations presented below. The new model uses an isotropic global diffusion tensor, \mathbf{R}^C . Since small deviations from spherical symmetry of the \mathbf{R}^C tensors of Hb A and HbCO A were reported previously,²⁰ we examine in Table 2 the sensitivity of ^{15}N T_1 , T_2 and $^{15}\text{N}-\{\text{H}\}$ NOE to \mathbf{R}^C axiality. A time scale separation of 10^{-3} , given by τ/τ_m , was used. For isotropic \mathbf{R}^C one has $\tau_m = 1/(6R^C)$, and for axial \mathbf{R}^C one has $\tau_m = 1/[2 \times (2R_{||}^C + R_{\perp}^C)]$. We used $c_0^2 = 10 k_B T$, which is typical of the local potentials determined for Hb A and HbCO A, and an isotropic local motional tensor, \mathbf{R}^L .

The correlation times for global motion, τ_m , were determined to be 32.8 and 29.0 (32.0 and 29.9) ns at 29 and 34 °C for Hb

A (HbCO A).²⁰ The ratio $R_{||}^C/R_{\perp}^C$ was determined to be 1.1, and the relative orientation of the principal axis of the \mathbf{R}^C tensor with respect to the inertia tensor frame of the relevant crystal structure was found to be given by $\Theta = 75.7^\circ$ and $\Phi = 190^\circ$, for Hb A and HbCO A at 29 and 34 °C.²⁰

Calculation 1 was carried out for isotropic \mathbf{R}^C . In calculation 2 we used the \mathbf{R}^C tensor determined in ref 20. Calculations 3 and 4 are analogous to calculation 2, except that $R_{||}^C/R_{\perp}^C$ was set equal to 1.5 and 2.0, respectively. In the last column on the right we show the percent difference between the relaxation parameters obtained with calculations 2–4, and the corresponding relaxation parameters obtained with calculation 1.

It can be seen that $R_{||}^C/R_{\perp}^C = 1.1$ has a negligible effect on the analysis: the percent differences between corresponding parameters associated with calculation 1 and 2 are within the experimental errors (given in the Supporting Information of ref 20). $R_{||}^C/R_{\perp}^C = 1.5$ has a significant effect on ^{15}N T_1 and T_2 . $R_{||}^C/R_{\perp}^C = 2.0$ has a substantial effect on all three relaxation parameters. We conclude that in this study \mathbf{R}^C may be taken to be isotropic.

3.2. HbA and HbCO A: SRLS Analysis. Figures 3–6 show the experimental ^{15}N relaxation data of Hb A and HbCO A obtained in previous work.²⁰ Experimental data associated with markedly outlying features (e.g., the $^{15}\text{N}-\{\text{H}\}$ NOE measured at 14.1 T, 29 °C, for residue G107 of the β -chain of Hb A; cf. Figure 4) were excluded from the analysis. ^{15}N T_1 and T_2 vary gradually as a function of magnetic field and temperature, as expected. The $^{15}\text{N}-\{\text{H}\}$ NOE values do not always vary gradually. In general, $^{15}\text{N}-\{\text{H}\}$ NOEs change as a function of magnetic field and temperature less (percentage-wise) than ^{15}N T_1 and T_2 (in view of the functional form of the $j_{K,K'}(\omega)$ functions, and the dependence of the NOE on high-frequency values of these functions); the accuracy with which they can

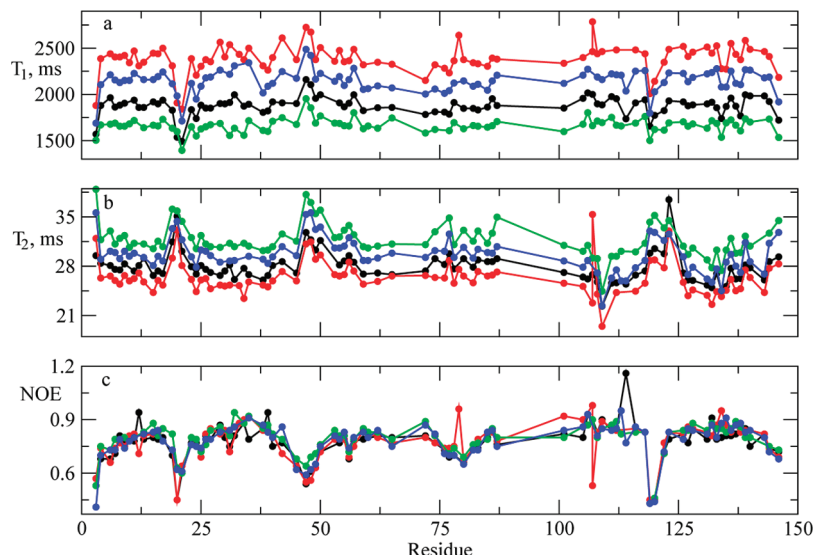


Figure 4. Experimental ^{15}N T_1 , T_2 and $^{15}\text{N}-\{\text{H}\}$ NOE acquired at 11.7 T and 29 °C (black), 14.1 T and 29 °C (red), 11.7 T and 34 °C (green), and 14.1 T and 34 °C (blue) for the β -chain of Hb A.²⁰

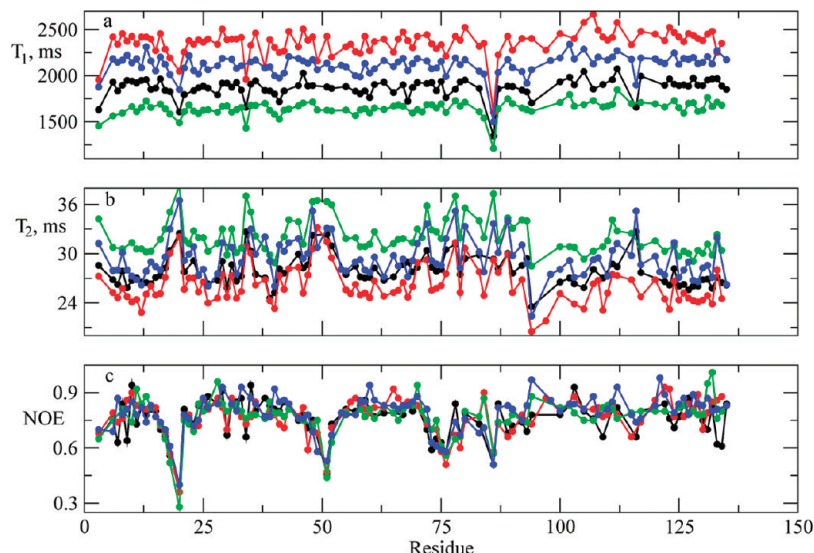


Figure 5. Experimental ^{15}N T_1 , T_2 and $^{15}\text{N}-\{\text{H}\}$ NOE acquired at 11.7 T and 29 °C (black), 14.1 T and 29 °C (red), 11.7 T and 34 °C (green), and 14.1 T and 34 °C (blue) for the α -chain of HbCO A.²⁰

be measured is often lower. To account for systematic and random experimental imperfections, the NOE errors were set uniformly to ± 0.03 .

The experimental data shown in Figures 3–6 were analyzed with the new model, where c_0^2 , R_L^L , β_D , and β_O are varied, and R_L^L is set equal to R^C . A simpler model consists of varying only c_0^2 and R^L and setting $\beta_D = \beta_O = 0$. This is the formal analogue of MF “model 2”,³⁸ we will use this designation below. The utilization of the new model instead of SRLS model 2 has to be justified. Figure 7 shows the results of applying both models to the experimental data of the α -chain of Hb A acquired at 11.7 and 14.1 T and 29 °C. The best-fit parameters generated by the new model are the black symbols/curves in parts a–d, representing S_0^2 (calculated from c_0^2), β_D , $\log(R_L^L)$, 1/s, and β_O , respectively. We show S_0^2 instead of c_0^2 because (1) in the strong ordering regime S_0^2 can be determined with higher accuracy than c_0^2 (see above), and (2) we wish to characterize the N–H sites consistently in terms of two tensors, S and R^L . The best-fit parameters generated by SRLS model 2 are the red symbols/curves in parts a and c, representing S_0^2 and $\log(R^L)$, 1/s,

respectively. The χ^2/df values associated with the new model (black) and SRLS model 2 (red) are shown in part e.

It can be seen that the red curve in part a comprises features displayed by the black curves in parts a and b. This indicates that S_0^2 of SRLS model 2 reflects in a nonseparable manner the structural information inherent in S_0^2 of the new model, and the geometric information inherent in β_D of the new model. As shown below, it also bears features of the local diffusion tensor. Part c of Figure 7 shows the local motional rates: the profiles of the new model (black) and SRLS model 2 (red) differ significantly.

The χ^2/df values associated with the new model are much smaller than the respective critical values (not shown). The red horizontal line in part e of Figure 7 shows the average of the 0.05 and 0.1 critical values of χ^2/df corresponding to the SRLS model 2 calculations. While most of the SRLS model 2 χ^2 values are below this threshold, they are much above it for the residues comprising the chain segment L100–R141. The S_0^2 values within this chain segment are unduly large and exhibit a trend similar to the β_O angles of the new model (part d).

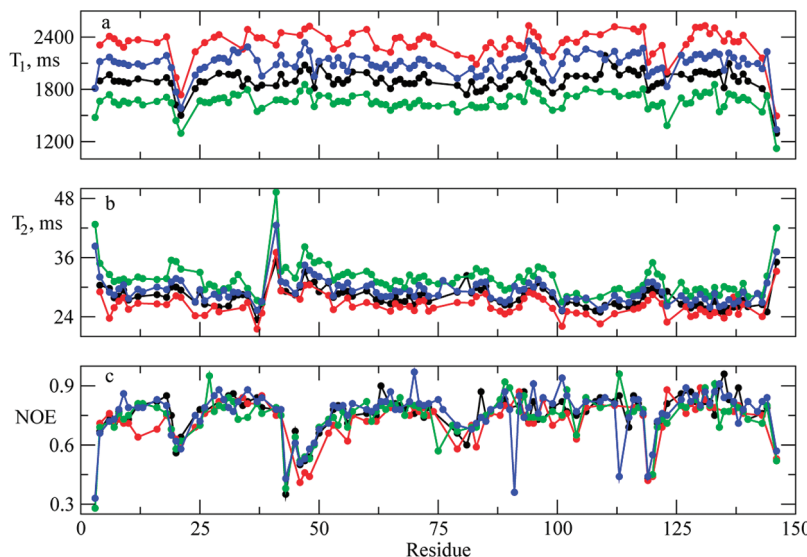


Figure 6. Experimental ^{15}N T_1 , T_2 and $^{15}\text{N}-\{^1\text{H}\}$ NOE acquired at 11.7 T and 29 °C (black), 14.1 T and 29 °C (red), 11.7 T and 34 °C (green), and 14.1 T and 34 °C (blue) for the β -chain of HbCO A.²⁰

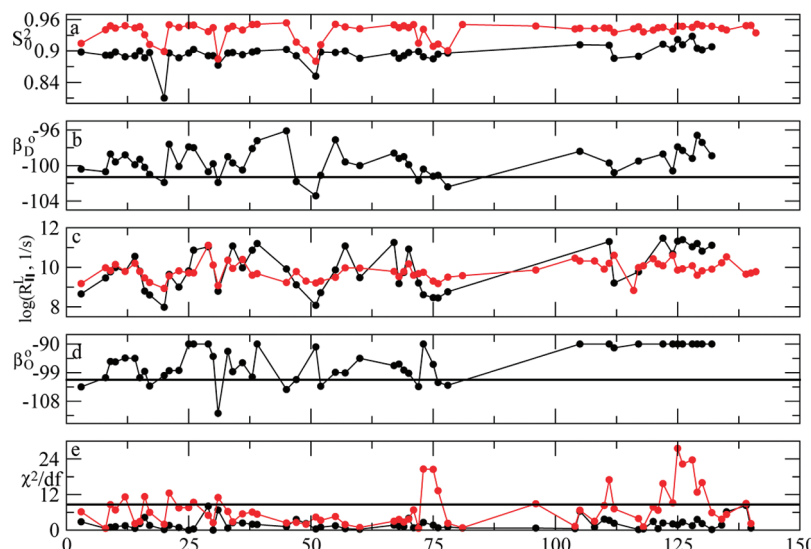


Figure 7. Best-fit values obtained for the experimental data acquired at 11.7 and 14.1 T, and 29 °C, for the α -chain of Hb A. Black: new model, where c_0^2 , R_{\perp}^L , β_D and β_O are allowed to vary, and $R_{\perp}^L = R^C$. Red: SRLS model 2, where c_0^2 and R^L are allowed to vary, and $\beta_D = \beta_O = 0$. Parts a, b, and d show S_0^2 , β_D and β_O , respectively. Part c shows $\log(R_{\parallel}^L, 1/\text{s})$ for the new model, and $\log(R_{\parallel}^L, 1/\text{s})$ for SRLS model 2. The horizontal line is the average of the 0.05 and 0.1 critical values for four degrees of freedom, corresponding to SRLS model 2. The errors are ± 0.015 in S_0^2 , $\pm 0.5^\circ$ in β_D , ± 0.15 in $\log(R_{\parallel}^L, 1/\text{s})$ and $\pm 2^\circ$ in β_O .

Clearly, the order parameters of SRLS model 2 are the result of experimental data having been force-fitted by an oversimplified model. This is a process where the statistical criteria are fulfilled, albeit with inaccurate parameters, which have absorbed unaccounted for factors. Except for the chain segment L100–R141, this has been accomplished with inaccurate (S_0^2)² values. Had R_{ex} been allowed to vary, the χ^2/df values of L100–R141 would have been also been acceptable, at the expense of artificial R_{ex} terms (this has been the scenario in the model-free analysis; cf. refs 20 and 34). Contrary to the oversimplified “SRLS model 2”, the new model accounts for the important factors within the scope of a physically sound analysis.

Figure 8 shows the S_0^2 profiles obtained with the new model (black), and SRLS model 2 (red) for the α -chain of Hb A acquired at 11.7 and 14.1 T, and 29 °C. It also shows the S^2 (green) and S (blue) profiles obtained with MF. All of these profiles represent the local ordering at N–H sites. However, they differ significantly from one another. Let us examine the

meaning of the various parameters depicted in Figure 8. In the classical theories for treating restricted motion in liquids (e.g., cf. refs 72 and 73 and papers cited therein), the local ordering is given by a tensor defined in terms of an ordering potential (eqs 3 and 4). For a potential $u(\Omega_{\text{CM}})$, with only the lowest $L = 2$ terms preserved (eq 3), the nonzero irreducible components are S_0^2 and S_2^2 , and the nonzero Cartesian components are S_{xx} , S_{yy} and S_{zz} (eq 4). The tensor S provides physically well-defined information on the preferential orientation of the local ordering frame in the local director frame. This constitutes important structural information.

The SRLS model 2 and the new model feature S_0^2 . As outlined above, S_0^2 of the SRLS model 2 is inaccurate. The MF spectral density³⁵ represents the SRLS limit for large time scale separation and an axial local ordering tensor collinear with the magnetic tensors.^{17–19} If these conditions are fulfilled, S will represent S_0^2 . If they are not fulfilled, as turned out to be the case,^{17–19} S will be inaccurate having absorbed important unaccounted for effects (the asymmetry of the local ordering^{18,19,39–44,47} and general

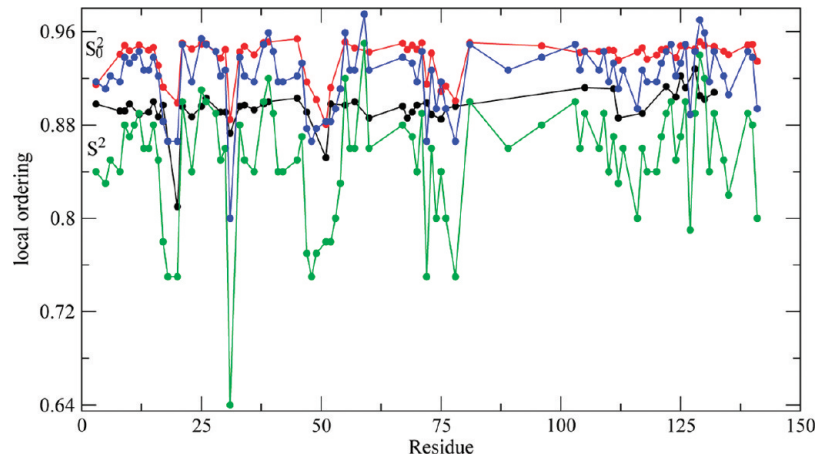


Figure 8. Local ordering information obtained with different analyses of the experimental data of the α -chain of Hb A acquired at 11.7 and 14.1 T, and 29 °C. Black: best-fit S_0^2 values obtained with the new model, where c_0^2 , R_{\parallel}^L , β_D , and β_O are allowed to vary, and $R_{\perp}^L = R^C$. Red: best-fit S_0^2 values obtained with SRLS model 2, where c_0^2 and R^L are allowed to vary, and $\beta_D = \beta_O = 0$. Green: best-fit S^2 values obtained with MF, and corresponding S values (blue).

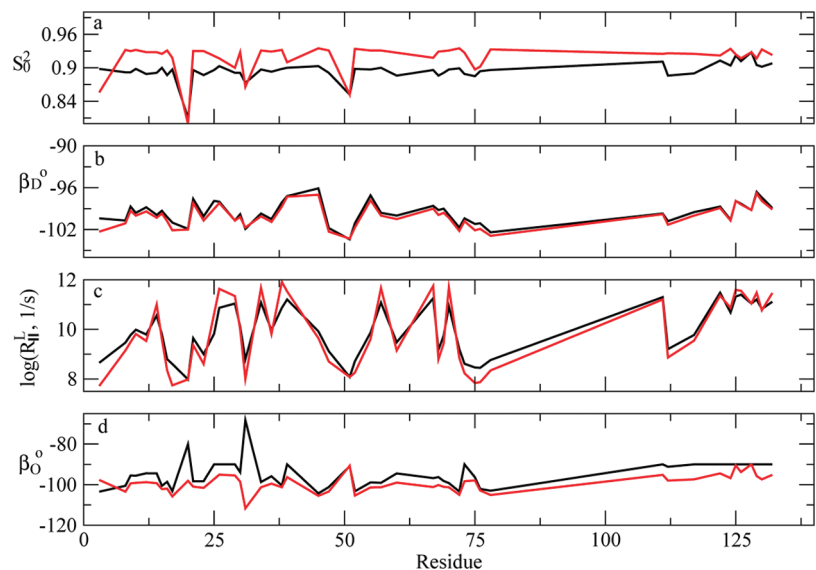


Figure 9. Best fit S_0^2 values obtained with the new model for the α -chain of Hb A (experimental data acquired at 11.7 and 14.1 T, and 29 °C) with $\beta_D = \beta_O = -101.3^\circ$ as starting values. The black curve corresponds to $c_0^2 = 10$ and $R_{\parallel}^L = 5.0 \times 10^9$ 1/s as starting values; the red curve corresponds to $c_0^2 = 15$ and $R_{\parallel}^L = 1.0 \times 10^{10}$ 1/s as starting values.

features of local geometry^{18,19,39–41,43,47}). Clearly, only the S_0^2 profile of the new model provides a physical description of the local ordering.

Let us examine the other parameters that enter the description of N–H bond dynamics. The new model provides a local diffusion tensor including principal values, $D_{2,\parallel}$ and $D_{2,\perp}$, and orientation, β_O . It has been shown that activation energies for local motion can be derived from the principal values of D_2 .^{48,49} The D_2 tensor is preset as isotropic in the SRLS model 2; MF uses the effective local motional correlation time, τ_e , which in view of its low accuracy was not even reported.²⁰ The sensitivity of the experimental data to the nonspherical symmetry of the D_2 tensor in a scenario where the S tensor is axially symmetric has been proven in this study.

The MF analysis used quite a few R_{ex} terms,²⁰ most of them turned out to be artificial, as Ho and co-workers showed more recently.³⁴ The SRLS model 2 had R_{ex} preset to zero; artificial R_{ex} terms would have improved the statistics within the chain segment L100–R141. The new model did not use R_{ex} contributions. The few residues for which R_{ex} was determined experimentally³⁴ will be further studied in future work.

Thus, the pictures yielded by MF and by the SRLS model 2 are poor approximations to the actual N–H bond dynamics in Hb A and HbCO A. On the other hand, the new model provides a comprehensive picture based on physically well-defined parameters; thereby it provides new insights.

Data sensitivity clearly justifies using the new model. The utilization of SRLS model 2 implies loss and distortion of information. Because four parameters are varied in the fitting process, the uncertainty in the best-fit parameters is larger in the new model than in SRLS model 2. However, it can be estimated by carrying out calculations for starting values of c_0^2 in the 10–15 range, and R_{\parallel}^L in the 5.0×10^9 to 1.0×10^{10} 1/s range. Figure 9 illustrates the range of the results obtained by applying the new model to the experimental data of the α -chain of Hb A acquired at 11.7 and 14.1 T, and 29 °C.²⁰ The results presented below (Figures 10–16) have been obtained with $c_0^2 = 10$ and $R_{\parallel}^L = 5.0 \times 10^9$ 1/s as starting values. On the basis of Figure 9, we estimate the $S_0^2(\beta_O)$ values obtained as lower limits of the $S_0^2(\beta_O)$ ranges; the upper limits are higher by 0.03 (-4°). The uncertainties in $\log(R_{\parallel}^L, 1/s)$ and β_D are ± 0.3 and -1.0° , respectively.

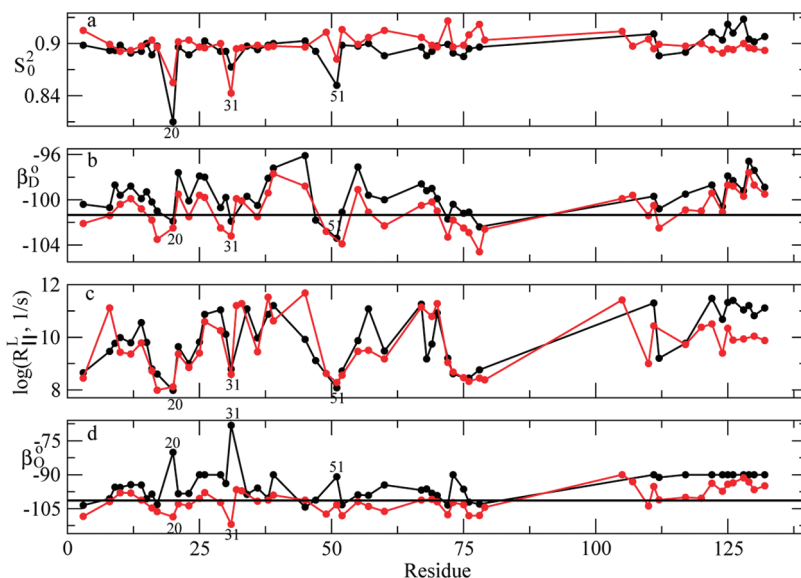


Figure 10. Best-fit parameters obtained by applying the new model to the experimental data the α -chain of Hb A acquired at 11.7 and 14.1 T, and 29 and 34 °C (Figure 3). S_0^2 is shown in part a, β_D in part b, $\log(R_{\parallel}^L, 1/s)$ in part c, and β_O in part d. The main flexible residues are demarcated. The errors are ± 0.015 in S_0^2 , $\pm 0.5^\circ$ in β_D , ± 0.15 in $\log(R_{\parallel}^L, 1/s)$, and $\pm 2^\circ$ in β_O .

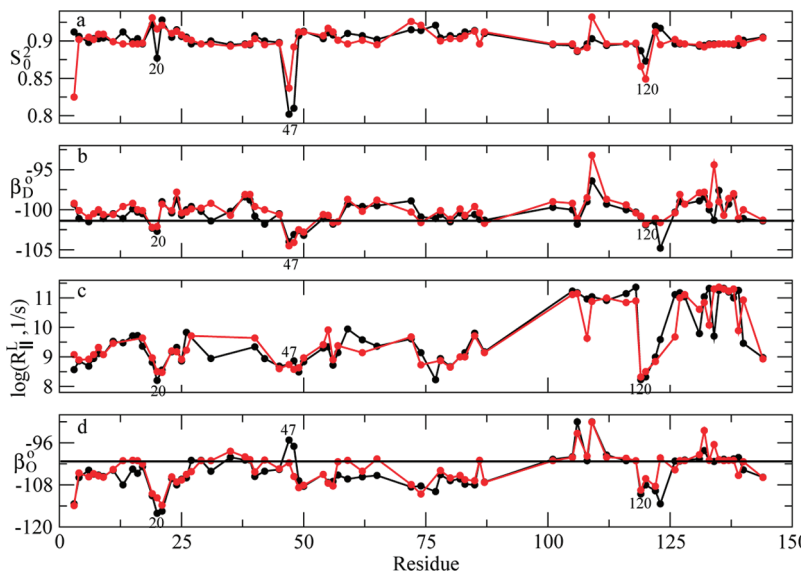


Figure 11. Best-fit parameters obtained by applying the new model to the experimental data the β -chain of Hb A acquired at 11.7 and 14.1 T, and 29 and 34 °C (Figure 4). S_0^2 is shown in part a, β_D in part b, $\log(R_{\parallel}^L, 1/s)$ in part c, and β_O in part d. The main flexible residues are demarcated. The errors are ± 0.015 in S_0^2 , $\pm 0.5^\circ$ in β_D , ± 0.15 in $\log(R_{\parallel}^L, 1/s)$, and $\pm 2^\circ$ in β_O .

Figures 10–13 show the results obtained for the α - and β -chains of Hb A and HBCO A. We analyzed N–H bonds for which data at 11.1 and 14.1 T, and 29 and 34 °C, are available for both the α - and β -chains. The χ^2/df values lie predominantly below the 0.05 critical value. A typical calculation for a given N–H bond took 350 s on a HP computer equipped with an Intel 2.7 GHz Dual Core CPU and 5GB of RAM.

The overall appearance of the patterns displayed by the best-fit parameters obtained with a physical fitting process should agree with the overall appearance of the patterns displayed by the experimental data. This is borne out quite well by Figures 10, 11, 12, and 13 in comparison with Figures 3, 4, 5, and 6. The agreement between the S^2 MF profile shown in Figure 8 and the Hb A profiles of Figure 3 is significantly less satisfactory. This can be realized by examining the various traces in Figure 10, which represent the best-fit parameters obtained for Hb A at 29 °C with the new model, and the corresponding experimental parameters shown in Figure 3. For practically every

outlier in Figure 3 (e.g., the NOEs of residues H20, G51, and D75), one can find one or several outliers among the four best-fit parameters depicted in Figure 10. As expected for physical data-fitting, experimental evidence is converted into well-defined physical parameters. On the other hand, the S^2 trace of Figure 8 exhibits quite a few outlying features which do not have counterparts in Figure 3. This is an indication of force-fitting.

Figure 10 shows the results obtained for the α -chain of Hb A at 29 and 34 °C; the corresponding experimental data are shown in Figure 3. For data of the rigid N–H bonds (associated with large $^{15}\text{N}-\{\text{H}\}$ NOEs in Figure 3) acquired at 29 °C the SRLS analysis yielded $S_0^2 = 0.9-0.93$, β_D values mostly more positive than -101.3° with an average deviation of 2° , $\log(R_{\parallel}^L, 1/s)$ on average 10, and β_O predominantly more positive than -101.3° with an average deviation of 4° . For data of the rigid N–H bonds acquired at 34 °C the SRLS analysis yielded similar S_0^2 and $\log(R_{\parallel}^L, 1/s)$ values. On the other hand, the local geometry

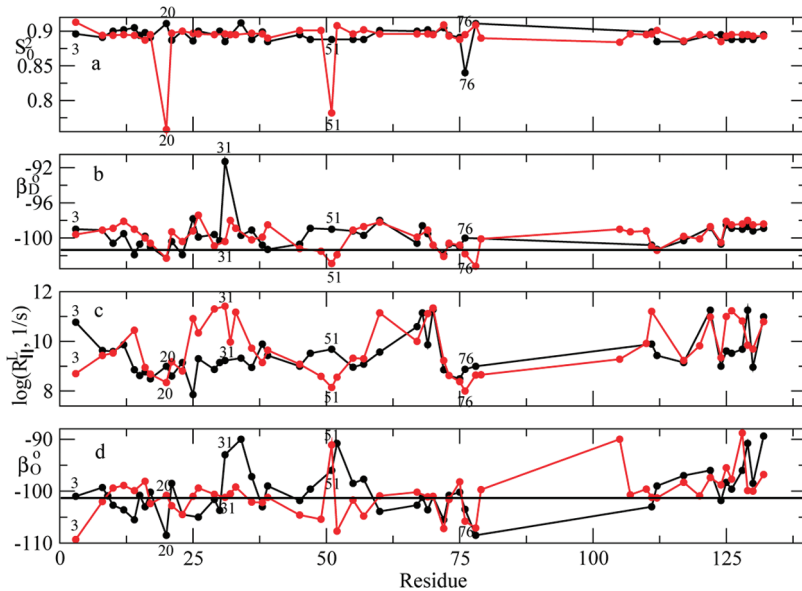


Figure 12. Best-fit parameters obtained by applying the new model to the experimental data the α -chain of HbCO A acquired at 11.7 and 14.1 T, and 29 and 34 °C (Figure 5). S_0^2 is shown in part a, β_D in part b, $\log(R_{\parallel}^L, 1/s)$ in part c, and β_O in part d. The main flexible residues are demarcated. The errors are ± 0.015 in S_0^2 , $\pm 0.5^\circ$ in β_D , ± 0.15 in $\log(R_{\parallel}^L, 1/s)$, and $\pm 2^\circ$ in β_O .

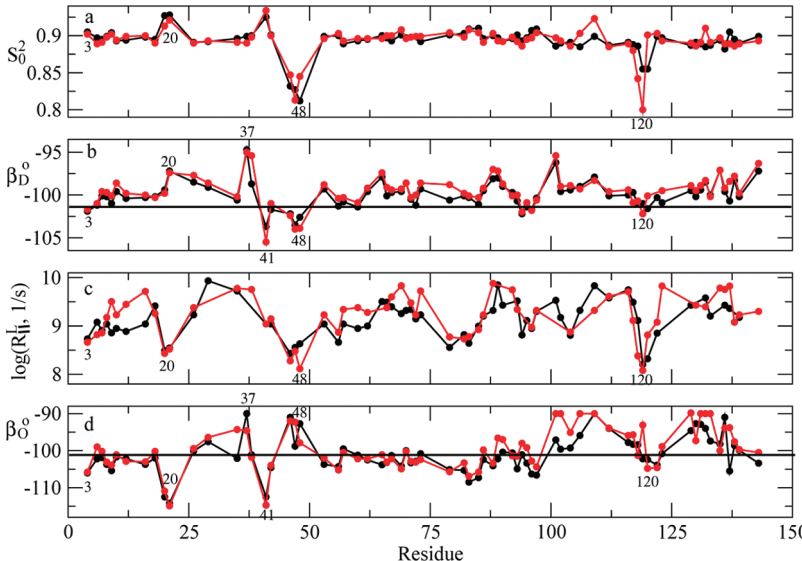


Figure 13. Best-fit parameters obtained by applying the new model to the experimental data the β -chain of HbCO A acquired at 11.7 and 14.1 T, and 29 and 34 °C (Figure 6). S_0^2 is shown in part a, β_D in part b, $\log(R_{\parallel}^L, 1/s)$ in part c, and β_O in part d. The main flexible residues are demarcated. The errors are ± 0.015 in S_0^2 , $\pm 0.5^\circ$ in β_D , ± 0.15 in $\log(R_{\parallel}^L, 1/s)$, and $\pm 2^\circ$ in β_O .

is different at the higher temperature, with both β_D and β_O being closer to -101.3° .

The residues in the chain segment L100–R141 pertain largely to the rigid N–H bond category. Here the best-fit parameters that correspond to 29 °C are conspicuously different from the best-fit parameters that correspond to 34 °C. At 29 °C the parameter S_0^2 is in the 0.90–0.93 range, while at 34 °C it is below 0.9. At both temperatures β_D is more positive than -101.3° , with the deviation at 29 °C exceeding the deviation at 34 °C. $\log(R_{\parallel}^L, 1/s)$ is approximately 11 at 29 °C and approximately 10 at 34 °C. The angle β_O assumes uniformly the value of -90° at 29 °C, and on average the value of -97° at 34 °C. These observations, and the distinction between the chain segments V1–D75 and L100–R141, require further investigation.

Let us examine the flexible N–H bonds of residues H20, R31, G51, and D75, associated with small $^{15}\text{N}-\{\text{H}\}$ NOEs in Figure 3. The best-fit parameters associated with these residues

differ significantly from those associated with the rigid residues. The local ordering is significantly weaker (smaller S_0^2); the principal axis of the local ordering tensor deviates from -101.3° in the opposite direction, i.e., toward more negative values. These deviations are larger at 29 °C (black). While the deviations from the value of -101.3° extend up to 2° for the rigid residues, they extend up to 4° for the flexible residues. The local motional rates are given by $\log(R_{\parallel}^L, 1/s)$ in the 8–8.3 range. At 29 °C the principal axis of the local diffusion tensor deviates from -101.3° toward more positive values; at 34 °C it deviates from -101.3° toward more negative values. While the deviations from -101.3° extend up to 4° for the rigid residues, they extend up to 10° for the flexible residues. Residue H20 is exceptional in having $\beta_O = -71^\circ$.

We review below Figures 11–13. Only exceptional features will be highlighted. Figure 11 shows the results obtained for the β -chain of Hb A at 29 and 34 °C. The rigid residues display

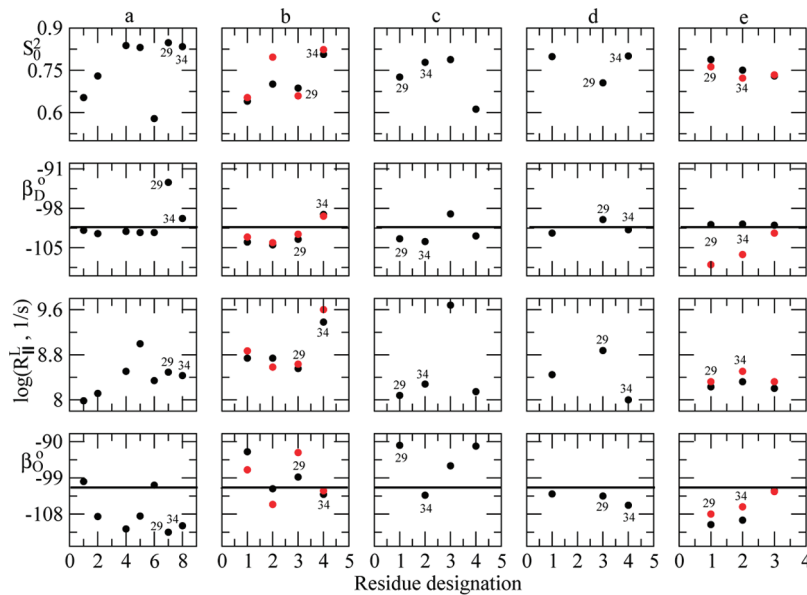


Figure 14. Best-fit parameters S_0^2 , β_D , $\log(R_{\parallel}^L, 1/s)$, and β_O obtained for residue 20 (H in the α -chain and V in the β -chain) (part a); residues $\alpha 47$ (D) (black) and $\alpha 48$ (L) (red) (part b); residue $\alpha 51$ (G) (part c); residue $\beta 76$ (A) (part d); and residues $\beta 120$ (K) (black) and $\beta 121$ (E) (red) (part e). The numbers 1–8 on the abscissa of part a signify Hb- α -29°, Hb- α -34°, Hb- β -29°, Hb- β -34°, HbCO- α -29°, HbCO- α -34°, HbCO- β -29°, and HbCO- β -34°. The numbers 1–4 on the abscissa of part b signify Hb- α -29°, Hb- α -34°, HbCO- α -29°, and HbCO- α -34°. The numbers 1–4 on the abscissa of part c signify Hb- α -29°, Hb- α -34°, HbCO- α -29°, and HbCO- α -34°. The numbers 1–4 on the abscissa of part d signify Hb- β -29°, Hb- β -34°, HbCO- β -29°, and HbCO- β -34°. The numbers 1–3 on the abscissa of part e signify Hb- β -29°, Hb- β -34°, and HbCO- β -29°. The errors are ± 0.015 in S_0^2 , $\pm 0.5^\circ$ in β_D , ± 0.15 in $\log(R_{\parallel}^L, 1/s)$, and $\pm 2^\circ$ in β_O .

features similar to those of the rigid residues of the α -chain. The flexible residues will be discussed separately (cf. Figure 14 below). Similar to the α -chain, one can distinguish between the chain segments V1–L75 and E101–H146: the local motional rates are on average higher, and the β_O angle on average more positive, in the latter chain segment.

Figure 12 shows the results obtained for the α -chain of HbCO A at 29 and 34 °C. The exceptional feature here is that each flexible N–H bond is dominated by a different factor. For V20 the main factor is large deviation of β_O from -101.3° . For L31 the main factor is large deviation of β_D from -101.3° (however, see below). For A76 the main factor is weak local ordering. These features should be investigated further in future work.

Figure 13 shows the results for the experimental data of the β -chain of HbCO A acquired at 11.7 and 14.1 T, and 29 and 34 °C. The results are consistent with the experimental data (Figure 6) and the structural context. On the scales of Figure 13 one can distinguish between the results obtained at 29 and 34 °C. The annotation makes possible to follow in detail the unique features of the flexible residues.

In Figure 14 we show the results obtained for the (main) flexible N–H bonds of Hb A and HbCO A. The purpose of this figure is to enable convenient comparison among the best-fit parameters of the loop residues of the two Hb forms. Parts a, b, c, d, and e correspond to residues 20, $\alpha 47/\alpha 48$ (black/red), $\alpha 51$, $\beta 76$, and $\beta 120/\beta 121$ (black/red). The amino acid designations are $\alpha 47$ (D), $\alpha 48$ (L), $\alpha 51$ (G), $\beta 76$ (A), $\beta 120$ (K), and $\beta 121$ (E). Residue 20 is H in the α -chain and V in the β -chain. The meaning of the numbers on the abscissa is delineated in the caption of Figure 14.

The angle β_O is predominantly more negative than -101.3° for residues 20, $\beta 76$, $\beta 120$, and $\beta 121$, and predominantly more positive than -101.3° for residues $\alpha 47$, $\alpha 48$, and $\alpha 51$. This represents a significant difference in the orientation of the local diffusion frame with respect to the N–H bond. The pairs labeled 29 and 34 illustrate the effect of the temperature. The trends in S_0^2 and $\log(R_{\parallel}^L, 1/s)$ in part e are expected: decrease in the local

ordering and increase in the local motional rate upon increasing the temperature. In general, one has to consider both the principal values and the orientations of the local ordering and local diffusion tensors in rationalizing the temperature-induced (or any other) changes.

We relate now to the residues that are particularly important from a structural/functional point of view. Residue $\beta 3$ (L) of Hb A has $S_0^2 \sim 0.9$, $\beta_D \sim -99.5^\circ$, $\log(R_{\parallel}^L, 1/s) \sim 9$, and $\beta_O \sim -105^\circ$. Residue $\beta 3$ of HbCO A has $S_0^2 \sim 0.9$, $\beta_D \sim -101.3^\circ$, $\log(R_{\parallel}^L, 1/s) \sim 8.3$ and $\beta_O \sim -105^\circ$. The differences between the two Hb A forms are relatively small for all the parameters. Residue $\beta 41$ (F) of the Hb A form has rigid-like parameters; the angles β_D and β_O are close to -101.3° . Residue $\beta 41$ of the HbCO A form has $\beta_D = -105^\circ$ and $\beta_O = -115^\circ$, indicating that the local geometry is significantly different from that prevailing in Hb A.

Experimental data for the residues $\beta 109$ (V), $\beta 123$ (T), and $\beta 146$ (H) are not available for the α -chain; hence they are not included in Figures 10–13. We analyzed them separately for the β -chain and obtained the following results. For residue $\beta 109$, the results are quite similar for Hb A and HbCO A at both 29 and 34 °C. Upon CO-binding S_0^2 decreases from 0.94 to 0.93, β_D changes from -93.8° to -98.1° , and the local motion changes from being negligible in Hb A to being given by $\log(R_{\parallel}^L, 1/s) = 9.6$ in HbCO A; β_O remains -90° . The significant changes upon CO binding include slowing down of the local motion, and the local ordering axis approaching the $C_i^\alpha - C_i^\alpha$ axis by 4.3° .

For residue $\beta 123$ we convey the (more consistent) results obtained at 29 °C. Upon CO binding, S_0^2 decreases from 0.95 to 0.90, β_D changes from -104.7° to -100.1° , $\log(R_{\parallel}^L, 1/s)$ increases from 9.3 to 11, and β_O changes from -112.4° to -101.1° . The significant changes include a large increase in the rate of the local motion, and the large deviation of 11° of the principal axis of the local diffusion tensor from N–H becoming practically zero.

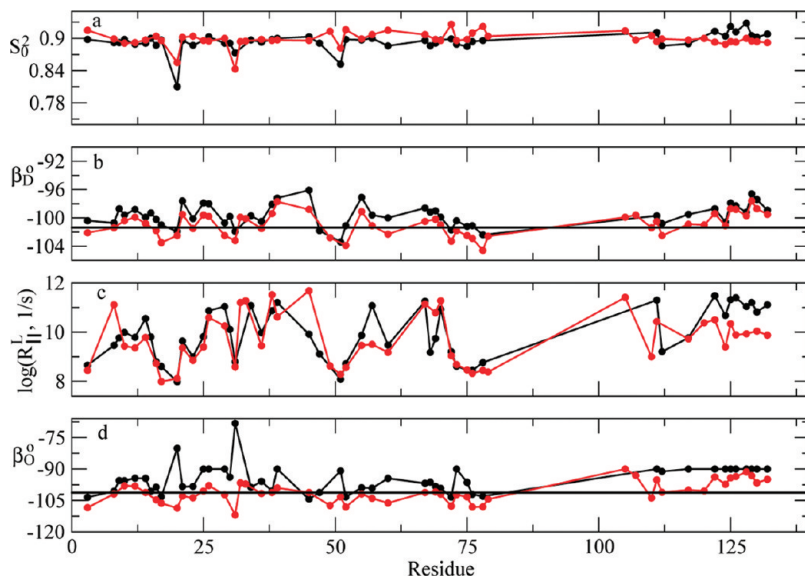


Figure 15. Best-fit parameters obtained with the new model for the α -chain of Hb A at 29 °C (black) and 34 °C (red). The errors are ± 0.015 in S_0^2 , $\pm 0.5^\circ$ in β_D , ± 0.15 in $\log(R_{\parallel}^L, 1/s)$, and $\pm 2^\circ$ in β_O .

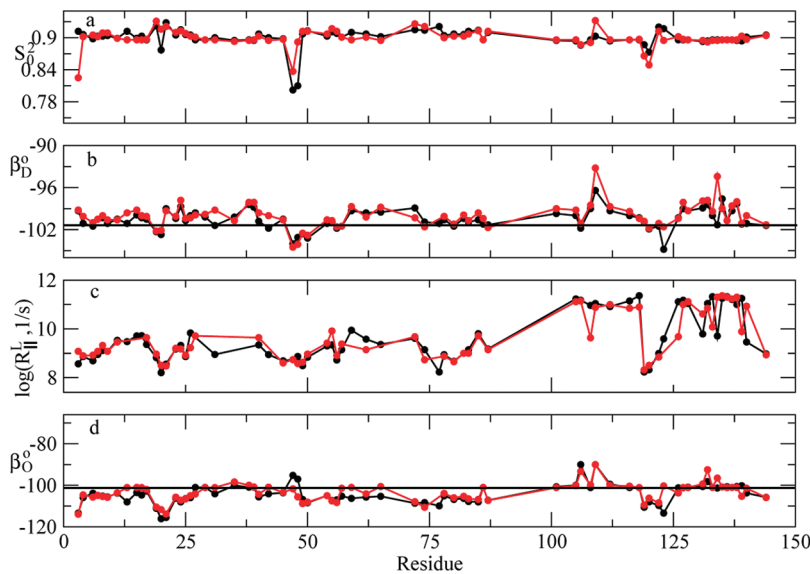


Figure 16. Best-fit parameters obtained with the new model for the β -chain of Hb A at 29 °C (black) and 34 °C (red), drawn on the same scales as used in Figure 15. The errors are ± 0.015 in S_0^2 , $\pm 0.5^\circ$ in β_D , ± 0.15 in $\log(R_{\parallel}^L, 1/s)$, and $\pm 2^\circ$ in β_O .

For residue $\beta 146$ we report the 34 °C results (because χ^2/df is 19.6 for HbCO A at 29 °C). The best-fit parameters are very similar for the two Hb forms. We found that $S_0^2 \sim 0.82$, $\beta_D \sim -101^\circ$, $\log(R_{\parallel}^L, 1/s) \sim 8.0$, and $\beta_O \sim -119^\circ$. As expected for an end-chain residue, S_0^2 is relatively small, the principal axis of the local ordering tensor is parallel to the $C_{i-1}^\alpha - C_i^\alpha$ axis, and the local motion is relatively slow. The principal axis of the local diffusion tensor deviates by 18° from the N–H bond. This is an unusually large deviation, which may be interpreted in terms of (expected) complex local motion.

Residue $\alpha 31$ (R) of the Hb A form has $S_0^2 \sim 0.85$, $\beta_D \sim -103^\circ$, and $\log(R_{\parallel}^L, 1/s) = 8.5$ at both temperatures; it has $\beta_O = -75^\circ$ at 29 °C and -108° at 34 °C. Residue $\alpha 31$ of the HbCO A form has $S_0^2 = 0.90$ at both temperatures; $\beta_D = -92^\circ$ at 29 °C and -98° at 34 °C, $\log(R_{\parallel}^L, 1/s) = 9$ at 29 °C and 11 at 34 °C, and $\beta_O = -90^\circ$ at 29 °C and -100° at 34 °C. These results are unusual both in terms of very large deviations from -101.3° in some cases and very large differences between 29 and 34 °C. Such (rare) cases require careful examination of the experimental data. Figure 10 shows that the $^{15}\text{N}-\{^1\text{H}\}$ NOEs of

residue $\alpha 31$ exhibit unusual trends. The expected trend is an increase in the NOE value both with increasing magnetic field, and with increasing temperature. Yet, the smallest NOE was measured at 14.1 T and 34 °C (blue), and the largest NOE was measured at 11.7 T and 29 °C (black). Figure 5 shows that for $\alpha 31$ of HbCO A the NOEs acquired at 29° are relatively small, whereas $^{15}\text{N} T_1$ and T_2 have common values. In all of the other cases, relatively small NOEs are accompanied by outstanding $^{15}\text{N} T_1$ and/or T_2 values. Residue $\alpha 31$ should be investigated further in future work.

The tensorial properties determined by the SRLS analysis depend on structural context of the N–H bond, the Hb form, and the temperature. They might be related to the (weak) forces which determine the quaternary structure of hemoglobin, and might be associated with the phenomenon of allostery. In the context of N–H bond dynamics “local flexibility” is often associated with “slower local motion”, with small $^{15}\text{N}-\{^1\text{H}\}$ NOEs as fingerprint. As shown herein, this concept is much broader in scope; it might connote structural (c_0^2, S_0^2), geometric (β_D, β_O), and kinetic (R_{\parallel}^L) information.

Figures 15 and 16 show the best-fit parameters obtained for the α - and β -chains of Hb A drawn on the same scales for convenient comparison. It can be seen that the differences between the results obtained at 29 and 34 °C are substantial for the α -chain and very small for the β -chain. The same holds true for the α - and β -chains of HbCO A (not shown). This observation is consistent with both forms of Hb prevailing in solution as ensembles of rapidly interconverting conformations. The following tentative interpretation is offered. The β -chains experience a broader distribution. An increase of 5° in the temperature implies a small shift in the population equilibrium, not captured by spin relaxation; therefore, the profiles in Figure 16 are almost indistinguishable at 29 and 34 °C. The α -chain is closer to a single conformation scenario, which is more sensitive to changes in temperature; the profiles in Figure 15 bear out these changes. Had Hb A and HbCO A prevailed as single-conformation structures, the α - and β -chains would have displayed similar temperature dependences. In general, these observations are consistent with the findings of refs 26 and 28. In particular, for HbCO A the prevalence of a conformational ensemble has been demonstrated quantitatively in the RDC study of ref 26. The MF analysis²⁰ is too inaccurate to capture this feature.

The new model appears to match the sensitivity of the experimental data. If the number of fitting parameters is decreased (e.g., by fixing β_D or β_O at -101.3°) or increased (e.g., by also allowing R_{\perp}^L to vary), the fitting process is impaired significantly.

4. Conclusions

The experimental ^{15}N relaxation parameters of the α - and β -chains of deoxy- and carbonmonoxy hemoglobin have been interpreted with SRLS in terms of an axial local ordering tensor and an axial local diffusion tensor tilted from one another. The principal axis of the local ordering tensor is (nearly) parallel to the $C_{i-1}^{\alpha}-C_i^{\alpha}$ axis; the principal axis of the local diffusion tensor is (nearly) parallel to the N–H bond. Hb A and HbCO A comprise mostly rigid N–H bonds which exhibit strong local ordering with S_0^2 of 0.88–0.95, and fast local motion with $R_{\parallel}^L \sim 10^9$ – 10^{10} 1/s. The deviation of the principal axis of the local ordering tensor from the $C_{i-1}^{\alpha}-C_i^{\alpha}$ axis is less than 2°; the deviation of the principal axis of the local diffusion tensor from the N–H bond is less than 4°. The flexible N–H bonds located in loops exhibit weaker ordering, with S_0^2 of 0.75–0.8, and slower local motion, with $R_{\parallel}^L \sim (1.0-6.3) \times 10^8$ 1/s. The deviation of the principal axis of the local ordering tensor from $C_{i-1}^{\alpha}-C_i^{\alpha}$ is less than 4°; the deviation of the principal axis of the local diffusion tensor from the N–H bond is less than 10°.

Interesting mesoscopic insights have been gained. Both rigid and flexible N–H bonds have been described within the scope of the same parameter combination. Virtually all the N–H bonds for which sufficient data are available have been described in terms of well-defined tensorial properties. There is clear distinction among structural, geometric, and dynamic characteristics. Unique features of the chain segment L100–R141 have been singled out. Temperature-induced changes that might indicate that the conformational distribution in solution is broader for the β -chains than for the α -chains have been detected. Additional insights are expected by combining the mesoscopic SRLS/NMR spin relaxation analysis with atomistic information provided by MD simulations.

These results are important in view of their physical clarity, inherent potential for further interpretation, consistency, and new

qualitative assessments. The SRLS-based picture supersedes considerably the model-free-based picture in the insights it provides.

Abbreviations. CSA, chemical shift anisotropy; Hb A, deoxy normal human adult hemoglobin; HbCO A, carbonmonoxy normal human adult hemoglobin; MD, molecular dynamics; MF, model-free; NMR, nuclear magnetic resonance; NOE, nuclear Overhauser enhancement; POMT, potential of mean torque; RDC, residual dipolar coupling; SRLS, slowly relaxing local structure.

Acknowledgment. The authors gratefully acknowledge Prof. Chien Ho of the Department of Biological Sciences, Carnegie Mellon University, Pittsburgh, PA, for help, support, advice, and the results of previous model-free analyses of Hb A and HbCO A. This work was supported by the Israel Science Foundation (Grant No. 347/07 to E.M.), the Binational Science Foundation (Grant No. 2006050 to E.M. and J.H.F.), the German-Israeli Science Foundation for Scientific Research and Development, grant no. 928-190.0/2006, and the Damadian Center for Magnetic Resonance at Bar-Ilan University, Israel (E.M.). This work was also supported by the National Center for Research Resources of the National Institutes of Health (Grant No. P41-RR016292 to J.H.F.). A.P. acknowledges support provided by Ministero dell'Istruzione, Universita e Ricerca (MIUR), grant PRIN 2008, and by the University of Padova, grant "Progetto Strategico" HELIOS 2009. E.M. gratefully acknowledges the hospitality of the Department of Computational and Systems Biology, University of Pittsburgh School of Medicine, where she spent her sabbatical year 2009/2010, in the course of which this work was carried out.

References and Notes

- Ishima, R.; Torchia, D. A. *Nat. Struct. Biol.* **2000**, *7*, 740.
- Case, D. A. *Acc. Chem. Res.* **2002**, *35*, 325.
- Brüschweiler, R. *Curr. Opin. Struct. Biol.* **2003**, *13*, 175.
- Palmer, A. G. *Chem. Rev.* **2004**, *104*, 3623.
- Mittermaier, A.; Kay, L. E. *Science* **2006**, *312*, 224.
- Igumenova, T. I.; Frederick, K. K.; Wand, A. J. *Chem. Rev.* **2006**, *106*, 1672.
- Kitao, A.; Wagner, G. *Magn. Reson. Chem.* **2006**, *44*, S130.
- Jarymowycz, V. A.; Stone, M. J. *Chem. Rev.* **2006**, *106*, 1624.
- Node, G.; Abergel, D. *Eur. Biophys. J. Biophys. Lett.* **2007**, *36*, 985.
- Markwick, P. R. L.; Malliavin, T.; Nilges, M. *PLoS Comput. Biol.* **2008**, *4*, 1.
- Muhandiram, D. R.; Yamazaki, T.; Sykes, B. D.; Kay, L. E. *J. Am. Chem. Soc.* **1995**, *117*, 11536.
- Millet, O.; Muhandiram, D. R.; Skrynnikov, N. R.; Kay, L. E. *J. Am. Chem. Soc.* **2002**, *124*, 6439.
- Srynnikov, N. R.; Millet, O.; Kay, L. E. *J. Am. Chem. Soc.* **2002**, *124*, 6449.
- Polimeno, A.; Freed, J. H. *Adv. Chem. Phys.* **1993**, *83*, 89.
- Polimeno, A.; Freed, J. H. *J. Phys. Chem.* **1995**, *99*, 10995.
- Liang, Z.; Freed, J. H. *J. Phys. Chem. B* **1999**, *103*, 6384.
- Tugarinov, V.; Liang, Z.; Shapiro, Yu. E.; Freed, J. H.; Meirovitch, E. *J. Am. Chem. Soc.* **2001**, *123*, 3055.
- Meirovitch, E.; Shapiro, Yu. E.; Polimeno, A.; Freed, J. H. *J. Phys. Chem. A* **2006**, *110*, 8366.
- Meirovitch, E.; Shapiro, Yu. E.; Polimeno, A.; Freed, J. H. *Prog. NMR Spectrosc.* **2010**, *56*, 360.
- Song, X.-J.; Yuan, Y.; Simplicianu, V.; Sahu, S. C.; Ho, N. Y.; Ho, C. *Biochemistry* **2007**, *46*, 6795.
- Dickerson, R. E.; Geis, I. *Hemoglobin: structure, function, evolution, and pathology*; Benjamin-Cummings: Menlo Park, CA, 1983.
- Perutz, M. F. *Nature* **1970**, *228*, 726.
- Silva, M. M.; Rogers, P. H. *J. Biol. Chem.* **1992**, *267*, 17248.
- Safo, M. K.; Abraham, D. J. *Biochemistry* **2005**, *44*, 8347.
- Kavanaugh, J. S.; Rogers, P. H.; Arnone, A. *Biochemistry* **2005**, *44*, 6101.
- Lukin, J. A.; Kontaxis, G.; Simplicianu, V.; Yuan, Y.; Bax, A.; Ho, C. *Proc. Natl. Acad. Sci. U.S.A.* **2003**, *100*, 517.

- (27) Simpliceanu, V.; Lukin, J. A.; Fang, T.-Y.; Zou, M.; Hi, N. T.; Ho, C. *Biophys. J.* **2000**, *79*, 1146.
- (28) Sahu, S. C.; Simpliceanu, V.; Gong, Q.; Ho, N. T.; Glushka, J. G.; Prestegard, J. H.; Ho, C. *J. Am. Chem. Soc.* **2006**, *128*, 6290.
- (29) Sahu, S. C.; Simpliceanu, V.; Ho, N. T.; Giovanelli, J. L.; Ho, C. *J. Biomol. NMR* **2006**, *36*, 1.
- (30) Mihailescu, M.-R.; Russu, I. M. *Proc. Natl. Acad. Sci. U.S.A.* **2001**, *98*, 3773.
- (31) Chang, C.-K.; Simpliceanu, V.; Ho, C. *Biochemistry* **2002**, *41*, 5644.
- (32) Balakrishnan, G.; Tsai, C.-H.; Wu, Q.; Case, M. A.; Pevsner, A.; McLendon, G. L.; Ho, C.; Spiro, T. G. *J. Mol. Biol.* **2004**, *340*, 857.
- (33) Yuan, Y.; Simpliceanu, V.; Lukin, J. A.; Ho, C. *J. Mol. Biol.* **2002**, *321*, 863.
- (34) Sing, X.-J.; Simpliceanu, V.; Ho, N. T.; Ho, C. *Biochemistry* **2008**, *47*, 4907.
- (35) Lipari, G.; Szabo, A. *J. Am. Chem. Soc.* **1982**, *104*, 4546.
- (36) Lipari, G.; Szabo, A. *J. Am. Chem. Soc.* **1982**, *104*, 4559.
- (37) Clore, G. M.; Szabo, A.; Bax, A.; Kay, L. E.; Driscoll, P. C.; Gronenborn, A. M. *J. Am. Chem. Soc.* **1990**, *112*, 4989.
- (38) Mandel, A. M.; Akke, M.; Palmer III, A. G. *J. Mol. Biol.* **1995**, *246*, 144.
- (39) Bremer, T.; Bruschweiler, R. *J. Am. Chem. Soc.* **1997**, *119*, 6672.
- (40) Fadel, A. R.; Jin, D. Q.; Montelione, G. T.; Levy, R. M. *J. Biomol. NMR* **1995**, *6*, 221.
- (41) Clore, G. M.; Schwieters, C. D. *Biochemistry* **2004**, *43*, 10678.
- (42) Ulmer, T. S.; Ramirez, B. E.; Delaglio, F.; Bax, A. *J. Am. Chem. Soc.* **2003**, *125*, 9179.
- (43) Mannfors, B. E.; Mirkin, N. J.; Palmo, K.; Krimm, S. *J. Phys. Chem. A* **2003**, *107*, 1825.
- (44) Abergel, D.; Bodenhausen, G. *J. Chem. Phys.* **2004**, *121*, 761.
- (45) Shapiro, Yu. E.; Kahana, E.; Tugarinov, V.; Liang, Z.; Freed, J. H.; Meirovitch, E. *Biochemistry* **2002**, *41*, 6271.
- (46) Tugarinov, V.; Shapiro, Yu. E.; Liang, Z.; Freed, J. H.; Meirovitch, E. *J. Mol. Biol.* **2002**, *315*, 171.
- (47) Meirovitch, E.; Shapiro, Yu. E.; Tugarinov, V.; Liang, Z.; Freed, J. H. *J. Phys. Chem. B* **2003**, *107*, 9883.
- (48) Shapiro, Yu. E.; Meirovitch, E. *J. Phys. Chem. B* **2006**, *110*, 11519.
- (49) Shapiro, Yu. E.; Kahana, E.; Meirovitch, E. *J. Phys. Chem. B* **2009**, *113*, 12050.
- (50) Zerbetto, M.; Polimeno, A.; Meirovitch, E. *J. Phys. Chem. B* **2009**, *113*, 13613.
- (51) Sezer, D.; Freed, J. H.; Roux, B. *J. Chem. Phys.* **2008**, *128*, 5106.
- (52) Sezer, D.; Freed, J. H.; Roux, B. *J. Phys. Chem. B* **2008**, *112*, 11014.
- (53) Sezer, D.; Freed, J. H.; Roux, B. *J. Phys. Chem. B* **2008**, *112*, 5755.
- (54) Sezer, D.; Freed, J. H.; Roux, B. *J. Am. Chem. Soc.* **2009**, *131*, 2597.
- (55) Zerbetto, M.; Carlotto, S.; Polimeno, A.; Corvaja, C.; Franco, J.; Toniolo, C.; Formaggio, F.; Barone, V.; Cimino, P. *J. Phys. Chem. B* **2007**, *111*, 2668.
- (56) Carlotto, S.; Cimino, P.; Zerbetto, M.; Franco, L.; Corvaja, C.; Crisma, M.; Formaggio, F.; Toniolo, C.; Polimeno, A.; Barone, V. *J. Am. Chem. Soc.* **2007**, *129*, 11248.
- (57) Barone, V.; Polimeno, A. *Chem. Soc. Rev.* **2007**, *36*, 1724.
- (58) Barone, V.; Polimeno, A. *Phys. Chem. Chem. Phys.* **2006**, *8*, 4609.
- (59) Barone, V.; Brustolon, M.; Cimino, P.; Polimeno, A.; Zerbetto, M.; Zoleo, A. *J. Am. Chem. Soc.* **2006**, *128*, 15865.
- (60) Zerbetto, M.; Polimeno, A.; Kotsyubynskyy, D.; Ghalebani, L.; Kowalewski, J.; Meirovitch, E.; Olsson, U.; Widmalm, G. *J. Chem. Phys.* **2009**, *131*, 234501.
- (61) Polimeno, A.; Meirovitch, E.; Freed, J. H. Manuscript in preparation.
- (62) Cornilescu, G.; Bax, A. *J. Am. Chem. Soc.* **2000**, *122*, 10143.
- (63) Fushman, D.; Cowburn, D. *J. Biomol. NMR* **1999**, *13*, 139.
- (64) Moro, G. J.; Polimeno, A. *J. Chem. Phys.* **1997**, *107*, 7884.
- (65) Freed, H. J.; Nayem, A.; Ranavare, S. B. *The Molecular Dynamics of Liquid Crystals*; Luckhurst, G. R., Veracini, C. A., Eds.; Kluwer Academic Publishers: Amsterdam, 1994; pp 271–312.
- (66) Abragam, A. *Principles of Nuclear Magnetism*; Oxford University Press (Clarendon): London, 1961.
- (67) Peng, J. W.; Wagner, G. In *Methods in Enzymology*; James, T. L., Oppenheimer, N. J., Eds.; Academic Press: New York, 1994; Vol. 239, pp 563–595.
- (68) Barone, V.; Zerbetto, M.; Polimeno, A. *J. Comput. Chem.* **2009**, *30*, 2.
- (69) Brink, D. M.; Satchler, G. R. *Angular Momentum*; Clarendon Press: Oxford, UK, 1968.
- (70) Spiegel, M. R.; Liu, J. *Mathematical Handbook of Formulas and Tables*, 2nd ed.; Schaum's Outline Series; McGraw-Hill: New York, 1999; p 266.
- (71) Fushman, D.; Tjandra, N.; Cowburn, D. *J. Am. Chem. Soc.* **1998**, *120*, 10947.
- (72) Polnaszek, C. F.; Bruno, G. V.; Freed, J. H. *J. Chem. Phys.* **1973**, *58*, 3185.
- (73) Polnaszek, C. F.; Freed, J. H. *J. Phys. Chem.* **1975**, *79*, 2283.
- (74) Akke, M.; Bruschweiler, R.; Palmer III, A. G. *J. Am. Chem. Soc.* **1993**, *115*.
- (75) Li, Z.; Raychaudhuri, S.; Wand, A. *J. Protein Sci.* **1996**, *5*, 2647.
- (76) Yang, D.; Kay, L. E. *J. Mol. Biol.* **1996**, *263*, 369.
- (77) Xue, Y.; Pavlova, M. S.; Ryabov, Y. E.; Reif, B.; Skrynnikov, N. R. *J. Am. Chem. Soc.* **2007**, *129*, 6827.

JP107553J